Magnetic exchange interaction in a pair of orbitally degenerate ions: Magnetic anisotropy of $[Ti_2Cl_9]^{-3}$

J. J. Borrás-Almenar, J. M. Clemente-Juan, E. Coronado,[a] A. V. Palii,[b] and B. S. Tsukerblat[b]
Departamento de Química Inorgánica, Universidad de Valencia, C/Dr. Moliner 50, E-46100, Burjassot Valencia, Spain

(Received 14 April 2000; accepted 11 October 2000)

The theory of the kinetic exchange in a pair of orbitally degenerate ions developed by the authors [J. Phys. Chem. A **102**, 200 (1998)] is applied to the case of face-shared bioctahedral dimer (overall D_{3h}-symmetry). The effective kinetic exchange Hamiltonian is found for a $^2T_2-^2T_2$ system taking into account all relevant transfer pathways and charge-transfer crystal field states. The influence of different transfer integrals involved in the kinetic exchange on the energy pattern and magnetic properties of the system is examined. The role of other related interactions (trigonal crystal field, spin–orbit coupling) is also discussed in detail. Using the pseudoangular momentum representation and the technique of the irreducible tensor operators of R_3-group we give a general outlook on the nontrivial symmetry properties of the effective Hamiltonian for the D_{3h}-pair, and on the magnetic anisotropy arising from the orbital interactions specific for the case of orbital degeneracy. The magnetic properties of the binuclear unit $[Ti_2Cl_9]^{-3}$ in $Cs_3Ti_2Cl_9$ are discussed with a special emphasis on the magnetic anisotropy experimentally observed in this system. The existing exchange models for $[Ti_2Cl_9]^{-3}$ and the concept of the effective Hamiltonian are discussed in the context of the present study. © *2001 American Institute of Physics.* [DOI: 10.1063/1.1329892]

I. INTRODUCTION

In the case of orbital degeneracy of the constituent ions, the isotropic spin-Hamiltonian of the magnetic exchange (Heisenberg–Dirac–VanVleck, HDVV model) becomes invalid even as a zeroth order approximation. The effective exchange Hamiltonian cannot be expressed in terms of spin operators only and contains also operators acting within the orbital spaces of interaction ions. For the first time Khomskii and Kugel derived the kinetic exchange Hamiltonian for orbitally degenerate ions and considered the problem of the orbital ordering in solids (see the review paper of Khomskii and Kugel[1] and references therein). The theory of the kinetic exchange was developed by Drillon and Georges[2] and Leuenberger and Güdel.[3] Because of the lack in the use of symmetry arguments and simplifications in the energy spectrum of the charge transfer states the models so far considered prove to be restricted in their applicability to the real systems.

In our recent paper[4] we proposed a new approach to the problem of the kinetic exchange between orbitally degenerate multielectron transition metal ions. Our consideration takes into account explicitly complex energy spectrum of charge transfer crystal field states exhibited by the Tanabe–Sugano diagrams. Taking advantage from the symmetry arguments we have deduced the effective exchange Hamiltonian in its general form for an arbitrary overall symmetry of the dimer taking into account all relevant electron transfer pathways. The effective Hamiltonian was constructed in terms of spin-operators and standard orbital operators (cubic irreducible tensors). All parameters of the Hamiltonian incorporate physical characteristics of the magnetic ions in their crystal surroundings. In fact, they are expressed in terms of the relevant (in a given overall symmetry) transfer integrals and crystal field and Racah parameters for the constituent ions.

In the present paper we apply the effective Hamiltonian deduced[4] to the case of the face-shared bioctahedral $d^1(^2T_2)-d^1(^2T_2)$ dimer (D_{3h} overall symmetry). Trivalent titanium ions form these kind of well isolated dimers in the crystal structure of $Cs_3Ti_2Cl_9$ (Refs. 5, 6) and $Cs_3Ti_2Br_9$ (Ref. 7) whose magnetic and spectroscopic properties were a subject of the discussion for almost two decades.[4,8–12] One of the most spectacular features of the magnetic behavior of the $[Ti_2Cl_9]^{-3}$ entity is a significant magnetic anisotropy that clearly indicates the importance of the orbital interactions.[6] Since the proposed effective Hamiltonian takes into account all relevant orbital interactions, this relatively simple system exhibiting distinct qualitative peculiarities could be a good test for the theory based on the effective Hamiltonian. Here we will discuss the magnetic properties of $[Ti_2Cl_9]^{-3}$ taking into account also relevant one-center interactions, namely, spin–orbit coupling and local low-symmetry (trigonal) components of the crystal field.

We will show briefly how the effective Hamiltonian deduced by the authors[4] and adapted to the point group D_{3h} can be treated using the irreducible tensor operator technique in the R_3 group. This allows us to introduce a pseudoangular momentum representation that provides clear insight on the

[a]Electronic mail: eugenio.coronado@uv.es
[b]On leave from the Quantum Chemistry Department, Institute of Chemistry, Academy of Sciences of Moldova, MD-2028 Kishinev, Moldova.

role of orbital interactions in the magnetic anisotropy of the system and to reveal some nontrivial symmetry properties of the effective Hamiltonian. Taking advantage of the effective Hamiltonian approach combined with the irreducible tensor operator technique in R_3, we will consider also some general properties of the face-shared dimers, and will discuss the existing models of the kinetic exchange in such kinds of systems.

II. EXCHANGE HAMILTONIAN OF THE FACE-SHARED BIOCTAHEDRAL D_{3h} PAIR

We start from the general expression for the effective exchange Hamiltonian for a pair of the metal ions A and B possessing orbitally degenerate ground terms,[4]

$$\begin{aligned}\mathbf{H}_{\mathrm{ex}} = -2 \sum_{\Gamma_A\Gamma_B\Gamma'_A\Gamma'_B} \sum_{\gamma_A\gamma_B\gamma'_A\gamma'_B} \sum_{\Gamma\gamma} \sum_{\Gamma'\gamma'} \langle \Gamma\gamma|\Gamma_A\gamma_A\Gamma'_A\gamma'_A\rangle \\ \times\langle\Gamma'\gamma'|\Gamma_B\gamma_B\Gamma'_B\gamma'_B\rangle \mathbf{O}^A_{\Gamma\gamma}\mathbf{O}^B_{\Gamma'\gamma'} \\ \times[J^{(0)}_{\Gamma\Gamma'}(\Gamma_A\gamma_A,\Gamma_B\gamma_B,\Gamma'_A\gamma'_A,\Gamma'_B\gamma'_B) \\ + J^{(1)}_{\Gamma\Gamma'}(\Gamma_A\gamma_A,\Gamma_B\gamma_B,\Gamma'_A\gamma'_A,\Gamma'_B\gamma'_B)\mathbf{S}_A\mathbf{S}_B], \qquad (1)\end{aligned}$$

where $\Gamma_{A(B)}\gamma_{A(B)}$ are the symmetry labels for the magnetic orbitals connected by the transfer integrals $t(\Gamma_A\gamma_A,\Gamma_B\gamma_B)$, $\mathbf{O}^A_{\Gamma\gamma}$ and $\mathbf{O}^B_{\Gamma\gamma}$ are the irreducible cubic tensors of $\Gamma\gamma$-type acting in the orbital spaces of the magnetic ions, $\mathbf{S}_A$ and $\mathbf{S}_B$ are the full spin operators. The parameters of the effective Hamiltonian $J^{(k)}_{\Gamma\Gamma'}(\Gamma_A\gamma_A,\Gamma_B\gamma_B,\Gamma'_A\gamma'_A,\Gamma'_B\gamma'_B)$ are proportional to the products of the transfer integrals $t(\Gamma_A\gamma_A,\Gamma_B\gamma_B)t'(\Gamma'_A\gamma'_A,\Gamma'_B\gamma'_B)$ and depend on the crystal field and Racah parameters of the ions in their normal reduced and oxidized forms; the receipt for their evaluation is given in the paper by Borrás *et al.*[4] [in this paper $J^{(0)}_{\Gamma\Gamma'}(\cdots)$ and $J^{(1)}_{\Gamma\Gamma'}(\cdots)$ were denoted as $U(\cdots)$ and $J(\cdots)$, respectively].

The binuclear unit $[Ti_2Cl_9]^{-3}$ represents a face-shared ${}^2T_2(t_2)-{}^2T_2(t_2)$ cluster with D_{3h} overall symmetry.[6] The molecular structure of $[Ti_2Cl_9]^{-3}$ and the local coordinate systems associated with the metal ions in their local surroundings are shown in Fig. 1(a). Following the general consideration,[4] we will use the cubic one-site basis related to C_4 axes (tetragonal basis) defined as $\xi\propto yz$, $\eta\propto xz$, $\zeta\propto xy(T_2)$, $u\propto 3z^2-r^2$, $v\propto\sqrt{3}(x^2-y^2)(E)$, $\alpha\propto L_x$, $\beta\propto L_y$, $\gamma\propto L_z(T_1)$.

Figure 2 illustrates two different types of transfer integrals. The transfer integrals of the first type $t(\xi_A,\xi_B)=t(\eta_A,\eta_B)=t(\zeta_A,\zeta_B)\equiv t$ (diagonal transfer pathways) are shown in Fig. 2(a). Figure 2(b) shows off-diagonal transfer integrals, namely, $t(\xi_A,\eta_B)=t(\eta_A,\zeta_B)=t(\xi_A,\zeta_B)\equiv t'$.

In order to deduce the Hamiltonian for the D_{3h} system one should substitute into the general expression of the Hamiltonian [Eq. (1)] the Clebsch–Gordan coefficients and to choose a definite set of relevant transfer integrals. In order to adapt this Hamiltonian to the ${}^2T_2(t_2)-{}^2T_2(t_2)$ system one should restrict the set of transfer parameters to those of t_2-t_2-types. One has also to incorporate into the parameters

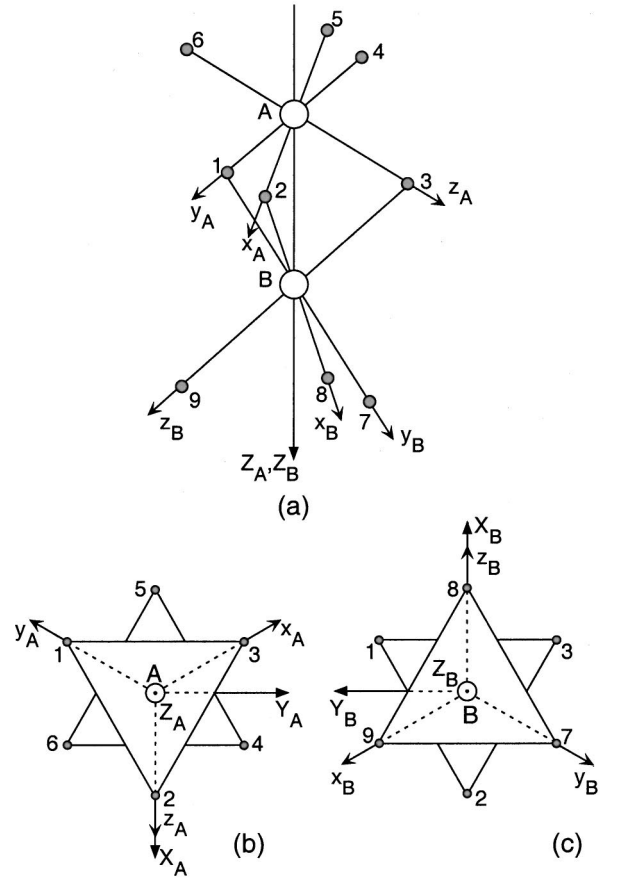

FIG. 1. Cartesian tetragonal and trigonal frames for a face-shared binuclear system: local tetragonal frames (a), local trigonal frames for the sites A (b) and B (c).

[Eq. (1)] the relationship between transfer integrals implied by D_{3h} symmetry. Then the Hamiltonian of the system can be presented as a sum of three terms,

$$\mathbf{H}=\mathbf{H}_t+\mathbf{H}_{t'}+\mathbf{H}_{tt'}. \qquad (2)$$

The first term of the Hamiltonian involving the diagonal transfer integrals is of the following form:

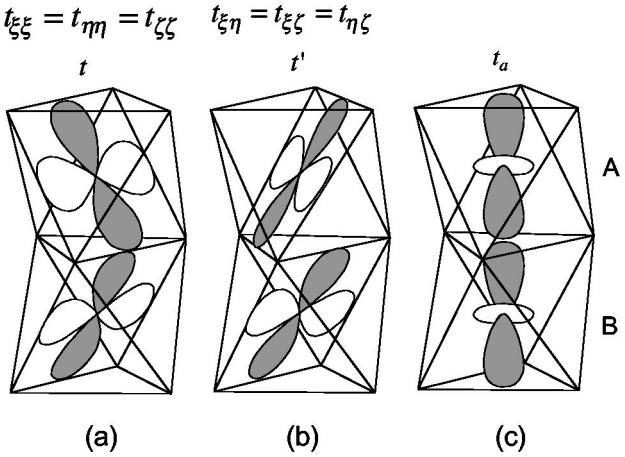

FIG. 2. Overlaps associated to different types of transfer integrals: diagonal transfer t(a), off-diagonal transfer t' (b), t_a transfer in trigonal basis (c).

$$\mathbf{H}_t = -2t^2\{F_E^{(0)}(\mathbf{O}_u^A\mathbf{O}_u^B+\mathbf{O}_v^A\mathbf{O}_v^B)+F_{T_1}^{(0)}(\mathbf{O}_\alpha^A\mathbf{O}_\alpha^B+\mathbf{O}_\beta^A\mathbf{O}_\beta^B+\mathbf{O}_\gamma^A\mathbf{O}_\gamma^B)$$
$$+F_{T_2}^{(0)}(\mathbf{O}_\xi^A\mathbf{O}_\xi^B+\mathbf{O}_\eta^A\mathbf{O}_\eta^B+\mathbf{O}_\zeta^A\mathbf{O}_\zeta^B)+[F_{A_1}^{(1)}\mathbf{O}_{A_1}^A\mathbf{O}_{A_1}^B+F_E^{(1)}(\mathbf{O}_u^A\mathbf{O}_u^B+\mathbf{O}_v^A\mathbf{O}_v^B)$$
$$+F_{T_1}^{(1)}(\mathbf{O}_\alpha^A\mathbf{O}_\alpha^B+\mathbf{O}_\beta^A\mathbf{O}_\beta^B+\mathbf{O}_\gamma^A\mathbf{O}_\gamma^B)+F_{T_2}^{(1)}(\mathbf{O}_\xi^A\mathbf{O}_\xi^B+\mathbf{O}_\eta^A\mathbf{O}_\eta^B+\mathbf{O}_\zeta^A\mathbf{O}_\zeta^B)]\mathbf{S}_A\mathbf{S}_B\}. \tag{3}$$

The second term involves only off-diagonal transfer integrals,

$$\mathbf{H}_{t'} = 2t'^2\Big\{F_E^{(0)}(\mathbf{O}_u^A\mathbf{O}_u^B+\mathbf{O}_v^A\mathbf{O}_v^B)+F_{T_1}^{(0)}(\mathbf{O}_\alpha^A\mathbf{O}_\alpha^B+\mathbf{O}_\beta^A\mathbf{O}_\beta^B+\mathbf{O}_\gamma^A\mathbf{O}_\gamma^B)-F_{T_2}^{(0)}(\mathbf{O}_\xi^A\mathbf{O}_\xi^B+\mathbf{O}_\eta^A\mathbf{O}_\eta^B+\mathbf{O}_\zeta^A\mathbf{O}_\zeta^B)$$
$$-\frac{2}{\sqrt{6}}F_{A_1T_2}^{(0)}[(\mathbf{O}_\xi^A+\mathbf{O}_\eta^A+\mathbf{O}_\zeta^A)\mathbf{O}_{A_1}^B+\mathbf{O}_{A_1}^A(\mathbf{O}_\xi^B+\mathbf{O}_\eta^B+\mathbf{O}_\zeta^B)]+\frac{1}{\sqrt{3}}F_{ET_2}^{(0)}[(\mathbf{O}_\xi^A+\mathbf{O}_\eta^A-2\mathbf{O}_\zeta^A)\mathbf{O}_u^B+\mathbf{O}_u^A(\mathbf{O}_\xi^B+\mathbf{O}_\eta^B-2\mathbf{O}_\zeta^B)]\Big\}$$
$$+2t'^2\Big\{-F_{A_1}^{(1)}\mathbf{O}_{A_1}^A\mathbf{O}_{A_1}^B+F_E^{(1)}(\mathbf{O}_u^A\mathbf{O}_u^B+\mathbf{O}_v^A\mathbf{O}_v^B)+F_{T_1}^{(1)}(\mathbf{O}_\alpha^A\mathbf{O}_\alpha^B+\mathbf{O}_\beta^A\mathbf{O}_\beta^B+\mathbf{O}_\gamma^A\mathbf{O}_\gamma^B)-F_{T_2}^{(1)}(\mathbf{O}_\xi^A\mathbf{O}_\xi^B+\mathbf{O}_\eta^A\mathbf{O}_\eta^B+\mathbf{O}_\zeta^A\mathbf{O}_\zeta^B)$$
$$-\frac{2}{\sqrt{6}}F_{A_1T_2}^{(1)}[(\mathbf{O}_\xi^A+\mathbf{O}_\eta^A+\mathbf{O}_\zeta^A)\mathbf{O}_{A_1}^B+\mathbf{O}_{A_1}^A(\mathbf{O}_\xi^B+\mathbf{O}_\eta^B+\mathbf{O}_\zeta^B)]+\frac{1}{\sqrt{3}}F_{ET_2}^{(1)}[(\mathbf{O}_\xi^A+\mathbf{O}_\eta^A-2\mathbf{O}_\zeta^A)\mathbf{O}_u^B+\mathbf{O}_u^A(\mathbf{O}_\xi^B+\mathbf{O}_\eta^B-2\mathbf{O}_\zeta^B)]\Big\}\mathbf{S}_A\mathbf{S}_B. \tag{4}$$

Finally, the third term contains the product of two types of transfer integrals,

$$\mathbf{H}_{tt'} = -2tt'\Big\{\frac{4}{\sqrt{6}}F_{A_1T_2}^{(0)}[(\mathbf{O}_\xi^A+\mathbf{O}_\eta^A+\mathbf{O}_\zeta^A)\mathbf{O}_{A_1}^B+\mathbf{O}_{A_1}^A(\mathbf{O}_\xi^B+\mathbf{O}_\eta^B+\mathbf{O}_\zeta^B)]+\frac{1}{\sqrt{3}}F_{ET_2}^{(0)}[(\mathbf{O}_\xi^A+\mathbf{O}_\eta^A-2\mathbf{O}_\zeta^A)\mathbf{O}_u^B+\mathbf{O}_u^A(\mathbf{O}_\xi^B+\mathbf{O}_\eta^B-2\mathbf{O}_\zeta^B)]\Big\}$$
$$-2tt'\Big\{\frac{4}{\sqrt{6}}F_{A_1T_2}^{(1)}[(\mathbf{O}_\xi^A+\mathbf{O}_\eta^A+\mathbf{O}_\zeta^A)\mathbf{O}_{A_1}^B+\mathbf{O}_{A_1}^A(\mathbf{O}_\xi^B+\mathbf{O}_\eta^B+\mathbf{O}_\zeta^B)]$$
$$+\frac{1}{\sqrt{3}}F_{ET_2}^{(1)}[(\mathbf{O}_\xi^A+\mathbf{O}_\eta^A-2\mathbf{O}_\zeta^A)\mathbf{O}_u^B+\mathbf{O}_u^A(\mathbf{O}_\xi^B+\mathbf{O}_\eta^B-2\mathbf{O}_\zeta^B)]\Big\}\mathbf{S}_A\mathbf{S}_B. \tag{5}$$

In Eqs. (3)–(5) the transfer integrals are shown explicitly. That is why instead of the parameters $J_{\Gamma\Gamma'}^{(n)}(\Gamma_A\gamma_A,\Gamma_B\gamma_B,\Gamma'_A\gamma'_A,\Gamma'_B\gamma'_B)$ involved in the general Hamiltonian [Eq. (1)], we have introduced the parameters $F_{\Gamma\Gamma'}^{(n)}(\cdots)$ defined as follows:

$$J_{\Gamma\Gamma'}^{(n)}[(t_2\xi)_A(t_2\xi)_B(t_2\xi)_A(t_2\xi)_B]$$
$$=J_{\Gamma\Gamma'}^{(n)}[(t_2\eta)_A(t_2\eta)_B(t_2\eta)_A(t_2\eta)_B]$$
$$=J_{\Gamma\Gamma'}^{(n)}[(t_2\zeta)_A(t_2\zeta)_B(t_2\zeta)_A(t_2\zeta)_B]\equiv t^2F_{\Gamma\Gamma'}^{(n)},$$
$$J_{\Gamma\Gamma'}^{(n)}[(t_2\xi)_A(t_2\xi)_B(t_2\xi)_A(t_2\eta)_B]=tt'F_{\Gamma\Gamma'}^{(n)},$$
$$J_{\Gamma\Gamma'}^{(n)}[(t_2\xi)_A(t_2\eta)_B(t_2\xi)_A(t_2\eta)_B]=t'^2F_{\Gamma\Gamma'}^{(n)}. \tag{6}$$

We have denoted also $F_{\Gamma\Gamma}^{(n)}\equiv F_\Gamma^{(n)}$. Symbol Γ in Eqs. (3)–(5) is omitted in the notations of the matrices $\mathbf{O}_{\Gamma\gamma}^i$, and they are identified through the symbol γ for the basis, namely, $\mathbf{O}_{\Gamma\gamma}^i\equiv\mathbf{O}_\gamma^i$ with $\gamma=u,v$ for $\Gamma=E$, $\gamma=\xi,\eta,\zeta$ for $\Gamma=T_2$, and $\gamma=\alpha,\beta,\gamma$ for $\Gamma=T_1$. The matrices $\mathbf{O}_{\Gamma\gamma}^i$ are given in Appendix A.

The Hamiltonian (2) is valid for the many-electron face-shared ${}^{2S+1}T_2(t_2^n)-{}^{2S+1}T_2(t_2^n)$-dimers. It operates in the space of the states, $|\Lambda_A^g=T_2,\lambda_A^g\rangle|\Lambda_B^g=T_2,\lambda_B^g\rangle|S_A^gM_A^g\rangle|S_B^gM_B^g\rangle$ representing the direct products of the ground one-center orbital and spin states. In the case of Ti^{3+} ions $S_{A(B)}^g=1/2$ (the total spin $S=0,1$).

III. EXCHANGE HAMILTONIAN IN THE TRIGONAL BASIS

In the previous section we have deduced the effective Hamiltonian relating the operators to the local tetragonal coordinate systems. For the subsequent calculations and discussion it is convenient to introduce the trigonal local coordinate systems X_A,Y_A,Z_A and X_B,Y_B,Z_B with $Z_A(Z_B)$ axes directed along C_3, as shown in Figs. 1(b) and 1(c). The common (molecular) coordinate system is taken to be coincident with the local trigonal system X_A,Y_A,Z_A. We pass to the complex trigonal basis x_0,x_+,x_- for T_2, a_0,a_+,a_- for T_1 and u_+,u_- for E. The unitary transformations are given by the following matrices:[13]

$$\begin{array}{c} \\ \frac{1}{\sqrt{3}}\end{array}\begin{array}{c} \begin{array}{ccc} x_+(a_+) & x_-(a_-) & x_0(a_0) \end{array} \\ \begin{bmatrix} -\omega & \omega^* & 1 \\ -\omega^* & \omega & 1 \\ -1 & 1 & 1 \end{bmatrix} \end{array}\begin{array}{c} \\ \begin{matrix}\xi(\alpha)\\ \eta(\beta)\\ \zeta(\gamma)\end{matrix}\end{array}, \quad \omega=\exp\left(\frac{2\pi i}{3}\right),$$

$$\begin{matrix} & u_+ & u_- \\ \frac{1}{\sqrt{2}}\begin{bmatrix} -1 & 1 \\ -i & -i \end{bmatrix} & \begin{matrix} u \\ v \end{matrix} \end{matrix}, \tag{7}$$

where $*$ indicates the complex conjugation.

In the trigonal basis there are two transfer integrals allowed by the symmetry conditions: $t(x_0^A, x_0^B) \equiv t_a$ and $t(x_+^A, x_+^B) = t(x_-^A, x_-^B) \equiv t_e$. The t_a and t_e transfer integrals (we use the notations introduced in Ref. 10) connect a-type (x_0) and e-type ($x_\pm$) orbitals appearing under the trigonal splitting of the cubic t_2-manifold. a-type orbitals overlap along C_3-axis [Fig. 2(c)] while the e-type orbitals are in perpendicular planes to the C_3-axis. Using the transformation (7) for one-electron T_2-basis one can find the following relationship between the transfer integrals defined in trigonal and tetragonal bases,

$$t_a = t + 2t', t_e = t - t'. \tag{8}$$

In the subsequent discussion we will use both sets of transfer parameters. After some simple but cumbersome calculations one can express the Hamiltonian in the trigonal coordinates as a sum of three contributions,

$$\mathbf{H} = \mathbf{H}_a + \mathbf{H}_e + \mathbf{H}_{ae}. \tag{9}$$

The first term is proportional to t_a^2, the second one is proportional to t_e^2, and the third one contains the product $t_a t_e$. These three contributions are given by Eqs. (10), (11) and (12),

$$\mathbf{H}_a = -\tfrac{2}{3} t_a^2 \{ 2F^{(0)}_{T_2} \mathbf{O}^A_{x_0} \mathbf{O}^B_{x_0} + \sqrt{2} F^{(0)}_{A_1 T_2} (\mathbf{O}^A_{A_1} \mathbf{O}^B_{x_0} + \mathbf{O}^A_{x_0} \mathbf{O}^B_{A_1}) + [F^{(1)}_{A_1} \mathbf{O}^A_{A_1} \mathbf{O}^B_{A_1} + 2F^{(1)}_{T_2} \mathbf{O}^A_{x_0} \mathbf{O}^B_{x_0} + \sqrt{2} F^{(1)}_{A_1 T_2} (\mathbf{O}^A_{A_1} \mathbf{O}^B_{x_0} + \mathbf{O}^A_{x_0} \mathbf{O}^B_{A_1})] \mathbf{S}_A \mathbf{S}_B \}, \tag{10}$$

$$\begin{aligned} \mathbf{H}_e = \tfrac{2}{3} t_e^2 \{ & F^{(0)}_E (\mathbf{O}^A_{u_+} \mathbf{O}^B_{u_-} + \mathbf{O}^A_{u_-} \mathbf{O}^B_{u_+}) - 2F^{(0)}_{T_2} (-\mathbf{O}^A_{x_+} \mathbf{O}^B_{x_-} - \mathbf{O}^A_{x_-} \mathbf{O}^B_{x_+} + \mathbf{O}^A_{x_0} \mathbf{O}^B_{x_0}) - 3F^{(0)}_{T_1} \mathbf{O}^A_{a_0} \mathbf{O}^B_{a_0} + F^{(0)}_{T_2} \mathbf{O}^A_{x_0} \mathbf{O}^B_{x_0} \\ & + \sqrt{2} F^{(0)}_{A_1 T_2} (\mathbf{O}^A_{A_1} \mathbf{O}^B_{x_0} + \mathbf{O}^A_{x_0} \mathbf{O}^B_{A_1}) + \sqrt{2} F^{(0)}_{E T_2} (\mathbf{O}^A_{x_+} \mathbf{O}^B_{u_-} + \mathbf{O}^A_{x_-} \mathbf{O}^B_{u_+} + \mathbf{O}^A_{u_-} \mathbf{O}^B_{x_+} + \mathbf{O}^A_{u_+} \mathbf{O}^B_{x_-}) \\ & + [-2F^{(1)}_{A_1} \mathbf{O}^A_{A_1} \mathbf{O}^B_{A_1} + F^{(1)}_E (\mathbf{O}^A_{u_+} \mathbf{O}^B_{u_-} + \mathbf{O}^A_{u_-} \mathbf{O}^B_{u_+}) \\ & - 2F^{(1)}_{T_2} (-\mathbf{O}^A_{x_+} \mathbf{O}^B_{x_-} - \mathbf{O}^A_{x_-} \mathbf{O}^B_{x_+} + \mathbf{O}^A_{x_0} \mathbf{O}^B_{x_0}) - 3F^{(1)}_{T_1} \mathbf{O}^A_{a_0} \mathbf{O}^B_{a_0} + F^{(1)}_{T_2} \mathbf{O}^A_{x_0} \mathbf{O}^B_{x_0} + \sqrt{2} F^{(1)}_{A_1 T_2} (\mathbf{O}^A_{A_1} \mathbf{O}^B_{x_0} + \mathbf{O}^A_{x_0} \mathbf{O}^B_{A_1}) \\ & + \sqrt{2} F^{(1)}_{E T_2} (\mathbf{O}^A_{x_+} \mathbf{O}^B_{u_-} + \mathbf{O}^A_{x_-} \mathbf{O}^B_{u_+} + \mathbf{O}^A_{u_-} \mathbf{O}^B_{x_+} + \mathbf{O}^A_{u_+} \mathbf{O}^B_{x_-})] \mathbf{S}_A \mathbf{S}_B \}, \end{aligned} \tag{11}$$

$$\begin{aligned} \mathbf{H}_{ae} = \tfrac{2}{3} t_a t_e \{ & 2F^{(0)}_E (\mathbf{O}^A_{u_+} \mathbf{O}^B_{u_-} + \mathbf{O}^A_{u_-} \mathbf{O}^B_{u_+}) - 3F^{(0)}_{T_1} (-\mathbf{O}^A_{a_+} \mathbf{O}^B_{a_-} - \mathbf{O}^A_{a_-} \mathbf{O}^B_{a_+} + \mathbf{O}^A_{a_0} \mathbf{O}^B_{a_0}) - F^{(0)}_{T_2} (-\mathbf{O}^A_{x_+} \mathbf{O}^B_{x_-} - \mathbf{O}^A_{x_-} \mathbf{O}^B_{x_+} + \mathbf{O}^A_{x_0} \mathbf{O}^B_{x_0}) \\ & + 3F^{(0)}_{T_1} \mathbf{O}^A_{a_0} \mathbf{O}^B_{a_0} + F^{(0)}_{T_2} \mathbf{O}^A_{x_0} \mathbf{O}^B_{x_0} - \sqrt{2} F^{(0)}_{E T_2} (\mathbf{O}^A_{x_+} \mathbf{O}^B_{u_-} + \mathbf{O}^A_{x_-} \mathbf{O}^B_{u_+} + \mathbf{O}^A_{u_-} \mathbf{O}^B_{x_+} + \mathbf{O}^A_{u_+} \mathbf{O}^B_{x_-}) \\ & + [2F^{(1)}_E (\mathbf{O}^A_{u_+} \mathbf{O}^B_{u_-} + \mathbf{O}^A_{u_-} \mathbf{O}^B_{u_+}) - 3F^{(1)}_{T_1} (-\mathbf{O}^A_{a_+} \mathbf{O}^B_{a_-} - \mathbf{O}^A_{a_-} \mathbf{O}^B_{a_+} + \mathbf{O}^A_{a_0} \mathbf{O}^B_{a_0}) - F^{(1)}_{T_2} (-\mathbf{O}^A_{x_+} \mathbf{O}^B_{x_-} - \mathbf{O}^A_{x_-} \mathbf{O}^B_{x_+} + \mathbf{O}^A_{x_0} \mathbf{O}^B_{x_0}) \\ & + 3F^{(1)}_{T_1} \mathbf{O}^A_{a_0} \mathbf{O}^B_{a_0} + F^{(1)}_{T_2} \mathbf{O}^A_{x_0} \mathbf{O}^B_{x_0} - \sqrt{2} F^{(1)}_{E T_2} (\mathbf{O}^A_{x_+} \mathbf{O}^B_{u_-} + \mathbf{O}^A_{x_-} \mathbf{O}^B_{u_+} + \mathbf{O}^A_{u_-} \mathbf{O}^B_{x_+} + \mathbf{O}^A_{u_+} \mathbf{O}^B_{x_-})] \mathbf{S}_A \mathbf{S}_B \}. \end{aligned} \tag{12}$$

The orbital matrices $\mathbf{O}_{\Gamma\gamma}$ in the trigonal T_2 basis are given in Appendix B.

IV. THE PARAMETERS OF THE EXCHANGE HAMILTONIAN

Let us express the parameters $F^{(n)}_{\Gamma\Gamma'}$ involved in $\mathbf{H}_a, \mathbf{H}_e$, and $\mathbf{H}_{ae}$ in terms of the crystal field parameters Dq and Racah parameters A, B, C defining the energy spectrum of the constituent ions in their ground, oxidized and reduced configurations. In the case under consideration the charge-transfer configurations are $d_A^2 - d_B^0$ and $d_A^0 - d_B^2$ so that all relevant parameters A, B, C, and Dq are related to the d^2 ion. The ${}^3T_1(t_2^2, t_2 e)$, ${}^1E(t_2^2, e^2)$, ${}^1A_1(t_2^2, e^2)$, and ${}^1T_2(t_2^2, t_2 e)$ terms of the d^2 ion (reduced $\tilde{S}\tilde{\Gamma}$ states) should be taken into account. This is because only these charge transfer states can be mixed with the ground one by means of the $t_2^A \to t_2^B$ transfer processes that are allowed in the overall D_{3h} symmetry. In fact, considering for example the reduced state ${}^3T_2(t_2 e)$ one can see that this can be obtained from $t_2 - t_2$ ground configuration only via the $t_2 \to e$ transfer process that is irrelevant in the case of interest. By means of the procedure described in Ref. 1 we arrive at the following formula for $F^{(n)}_{\Gamma\Gamma'}$-parameters:

$$\begin{aligned} F^{(n)}_{\Gamma\Gamma'} = & N_1^{(n)}(\Gamma\Gamma') F_1 + N_2^{(n)}(\Gamma\Gamma') F_2 + N_3^{(n)}(\Gamma\Gamma') F_3 \\ & + N_4^{(n)}(\Gamma\Gamma') F_4, \end{aligned} \tag{13}$$

where $N_i^{(n)}(\Gamma\Gamma')$ are the numerical coefficients collected in Table I, the parameters F_i are defined by

$$F_1 = 2\left[\frac{\cos^2\delta}{\varepsilon_1({}^1T_2)} + \frac{\sin^2\delta}{\varepsilon_2({}^1T_2)}\right], \quad F_2 = 2\left[\frac{\cos^2\theta}{\varepsilon_1({}^3T_1)} + \frac{\sin^2\theta}{\varepsilon_2({}^3T_1)}\right], \tag{14}$$

$$F_3 = 2\left[\frac{\cos^2\alpha}{\varepsilon_1({}^1A_1)} + \frac{\sin^2\alpha}{\varepsilon_2({}^1A_1)}\right], \quad F_4 = 2\left[\frac{\cos^2\beta}{\varepsilon_1({}^1E)} + \frac{\sin^2\beta}{\varepsilon_2({}^1E)}\right].$$

TABLE I. The numerical factors $N_i^{(n)}(\Gamma\Gamma')$ in Eq. (13).

Γ	Γ'	i	$N_i^{(0)}(\Gamma\Gamma')$	$N_i^{(1)}(\Gamma\Gamma')$
A_1	A_1	1	1/12	$-1/3$
		2	1/4	1/3
		3	1/36	$-1/9$
		4	1/18	$-2/9$
E	E	1	$-1/12$	1/3
		2	$-1/4$	$-1/3$
		3	1/18	$-2/9$
		4	1/9	$-4/9$
T_1	T_1	1	$-1/8$	1/2
		2	3/8	1/2
		3	1/12	$-1/3$
		4	$-1/12$	1/3
T_2	T_2	1	1/8	$-1/2$
		2	$-3/8$	$-1/2$
		3	1/12	$-1/3$
		4	$-1/12$	1/3
A_1	T_2	1	$\sqrt{3}/16$	$-\sqrt{3}/4$
		2	$\sqrt{3}/16$	$1/4\sqrt{3}$
		3	$1/12\sqrt{3}$	$-1/3\sqrt{3}$
		4	$1/24\sqrt{3}$	$-1/6\sqrt{3}$
E	T_2	1	0	0
		2	$-\sqrt{3}/4\sqrt{2}$	$-1/\sqrt{6}$
		3	$1/6\sqrt{6}$	$-\sqrt{2}/3\sqrt{3}$
		4	$1/12\sqrt{6}$	$-1/3\sqrt{6}$

Each F_i parameter is associated with one kind of terms of the reduced ion. In Eq. (14) the angles θ, α, β, and δ are the functions of the crystal field and Racah parameters (Appendix C). These angles characterize the mixing of the repeating terms arising from the different strong cubic field configurations. The parameters F_i^{-1} play the same role in our consideration as the energy U in the Anderson's theory of the kinetic exchange. The energies of charge transfer states in the denominators in Eq. (14) contain the common term A and crystal field energies $\varepsilon'_\mu(\tilde{S}\tilde{\Gamma})$,

$$\varepsilon_\mu(\tilde{S}\tilde{\Gamma}) = A + \varepsilon'_\mu(\tilde{S}\tilde{\Gamma}), \tag{15}$$

where

$$\begin{aligned}
\varepsilon'_{1(2)}({}^3T_1) &= \tfrac{1}{2}\{10Dq - B \mp [(10Dq + 9B)^2 + 144B^2]^{1/2}\},\\
\varepsilon'_{1(2)}({}^1A_1) &= \tfrac{1}{2}\{20Dq + 9(2B + C) \mp [(20Dq - 2B - C)^2 \\
&\quad + 24(2B + C)^2]^{1/2}\},\\
\varepsilon'_{1(2)}({}^1E) &= \tfrac{1}{2}\{20Dq + B + 4C \mp [(20Dq - B)^2 \\
&\quad + 48B^2]^{1/2}\},\\
\varepsilon'_{1(2)}({}^1T_2) &= \tfrac{1}{2}\{10Dq + B + 4C \mp [(10Dq - B)^2 \\
&\quad + 48B^2]^{1/2}\}.
\end{aligned} \tag{16}$$

The energies in Eq. (15) are counted from the energies of the pair of noninteracting ${}^2T_2$-ions.

TABLE II. Orbital basis for the effective Hamiltonian (9) in the case of the ${}^2T_2$–${}^2T_2$ system and related terms. Upper (lower) function for orbital doublets E' and E'' corresponds to $u_+(u_-)$.

Terms	Symmetry adapted orbital basis
${}^3A_2'$, ${}^1A_1''$	$\frac{1}{\sqrt{2}}(x_-^A x_+^B - x_+^A x_-^B)$
[I] ${}^3A_2''$, ${}^1A_1'$	$\frac{1}{\sqrt{3}}(x_0^A x_0^B - x_-^A x_+^B - x_+^A x_-^B)$
[II] ${}^3A_2''$, ${}^1A_1'$	$\frac{1}{\sqrt{6}}(2x_0^A x_0^B + x_-^A x_+^B + x_+^A x_-^B)$
[I] ${}^3E''$, ${}^1E'$	$\frac{1}{\sqrt{3}}(x_+^A x_0^B + x_0^A x_+^B - x_-^A x_-^B)$
	$\frac{1}{\sqrt{3}}(x_+^A x_+^B + x_0^A x_-^B + x_-^A x_0^B)$
[II] ${}^3E''$, ${}^1E'$	$-\frac{1}{\sqrt{6}}(x_+^A x_0^B + x_0^A x_+^B + 2x_-^A x_-^B)$
	$\frac{1}{\sqrt{6}}(2x_+^A x_+^B - x_0^A x_-^B - x_-^A x_0^B)$
${}^3E'$, ${}^1E''$	$\frac{1}{\sqrt{2}}(x_0^A x_+^B - x_+^A x_0^B)$
	$\frac{1}{\sqrt{2}}(x_-^A x_0^B - x_0^A x_-^B)$

V. ENERGY LEVELS OF THE FACE-SHARED ${}^2T_2$–${}^2T_2$ BIOCTAHEDRON

The effective exchange Hamiltonian (9) can be diagonalized using the symmetry adapted two-center orbital basis. This basis and the corresponding terms of the face-shared ${}^2T_2$–${}^2T_2$ bioctahedron are given in Table II. The energy levels in terms of the parameters F_i and two transfer integrals t_a and t_e are given in Appendix D, along with the 2×2 matrices for the repeating terms $2\,{}^3A_2''({}^2A_1')$ and $2\,{}^3E''({}^2E')$. These energies and matrices contain also the trigonal crystal field terms that will be discussed below and contributions of the intersite Coulomb repulsion between unfilled electronic shells that will be briefly discussed in the context of their influence on the magnetic behavior.

In the calculations of the energy pattern we use the Racah parameters evaluated for the free Ti^{2+} ion by Clementi *et al.*,[14] namely, $A = 14\,100\ \mathrm{cm}^{-1}$, $B = 900\ \mathrm{cm}^{-1}$, $C = 3300\ \mathrm{cm}^{-1}$ (these values are close to those found in the crystal field[13]). An independent estimation of A can be found comparing the ionization potentials for the configurations Ti^{+2}–Ti^{+3} (2.6525 MJ/mol) and Ti^{+3}–Ti^{+4} (4.1746 MJ/mol).[15] This estimation gives $A = 15.03$ eV that is close to the value calculated for the free Ti^{+2} ion. Similar estimation can be obtained from the formula $A = F_0 - 49F_{10}$ (Ref. 13) with the Slater–Condon parameters expressed in terms B and C by the use of Eq. (5.3) of Tanabe–Sugano's book.[13] The cubic field splitting parameter Dq is taken to be Dq

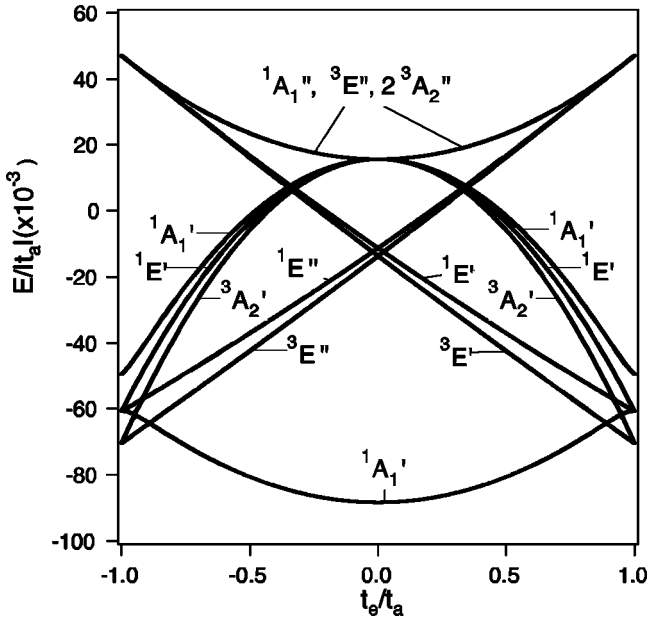

FIG. 3. Energy pattern of the face-shared ${}^2T_2-{}^2T_2$ system as a function of t_e/t_a.

$=1000\,\mathrm{cm}^{-1}$ that is typical for divalent metal ions[13] (reduced ion in the case under consideration).

Figure 3 shows the energy levels as a function of the ratio t_e/t_a in the range $-1\leqslant t_e/t_a\leqslant 1$. One can see that the energy pattern is symmetric with respect to the change of the sign of t_e/t_a. In a wide range of t_e/t_a the ground state is the spin singlet ${}^1A_1'$. Only at $t_e/t_a>0.9(t_e/t_a<-0.9)$ the orbital doublet ${}^3E'({}^3E'')$ becomes the ground state. The highest excited state is accidentally degenerate and comprises several multiplets, mainly spin-triplets. It is to be noted that the full gap of exchange splitting (except terminal parts of the diagram) is almost independent of the ratio t_e/t_a and mainly depends on t_a.

Three special high-symmetric cases are seen in Fig. 3, namely:

(i) Pseudospherical case: $t_e/t_a=1$ $(t_a=t_e=t,t'=0)$;
(ii) Spherical case: $t_e/t_a=-1$ $(t=-t_a/3,t'=-2t)$;
(iii) Axial case: $t_e/t_a=0$ $(t=t'=t_a/3)$.

In each of these cases the energy pattern exhibits a high degree of accidental degeneracy that shows that the effective Hamiltonian belongs to a more general symmetry group than the point symmetry group D_{3h}. The reasons for the use of terms pseudospherical, spherical and axial will be clarified below in the context of the discussion of the magnetic characteristics.

Let us consider first the cases (i) and (ii). Since the diagram is symmetric, the energy patterns for spherical and pseudospherical limits are the same. This is depicted in Fig. 4, where the terms are shown for cases (i) and (ii) in the left and right sides, correspondingly. One can see that the energy gaps in these two cases are determined by four parameters, J_i, related to the parameters F_i by

$$J_1=-t_a^2F_1,\quad J_2=t_a^2F_2,\quad J_3=-t_a^2F_3,\quad J_4=-t_a^2F_4. \tag{17}$$

It should be noted that the parameters J_1 and J_4 are very close due to the fact that ${}^1E$ and ${}^1T_2$ reduced states are almost degenerate in a wide range of Dq/B values with the exception of a narrow region of weak crystal field (see the Sugano–Tanabe diagram for d^2).[13] Therefore the splitting of the first excited group of levels is also very small ($\approx 0.01\,\mathrm{cm}^{-1}$ for a reasonable set of parameters). This gap is

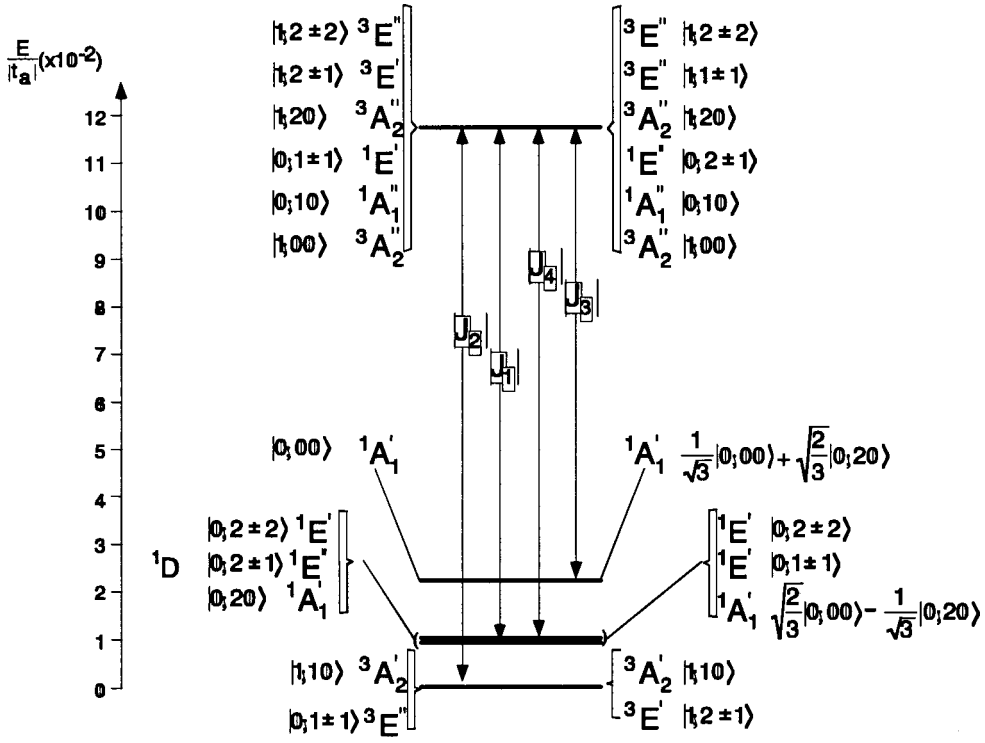

FIG. 4. Energy pattern of the face-shared ${}^2T_2-{}^2T_2$ system in the spherical (left-side labels) and pseudospherical (right-side labels) limits.

artificially increased in Fig. 4. Since this small splitting does not affect the magnetic properties, we will consider in the following that the first excited group contains degenerate levels.

For the subsequent discussion it is very useful to pass to the angular momentum representation applying the irreducible tensor operators technique for the R_3-group.[16–22] The full description of this new approach and its applications will be published elsewhere.[23] Here we will mention concisely only the main ideas and results that will be used in the present discussion. In the **O**-group three cyclic components of the orbital angular momentum operator, namely, $L_{10}=L_Z$ and $L_{1\pm1}=\mp(1/\sqrt{2})(L_X\pm iL_Y)$ quantizied along the C_3 axis form the trigonal basis of T_1 and the matrices $\mathbf{O}_{T_1\gamma}$ are related to the matrices of L_{1q} with $L=1$ ($T-P$ isomorphism or $T-P$ analogy) as follows:

$$\mathbf{O}_{a_0}=\frac{i}{\sqrt{2}}L_{10},\quad \mathbf{O}_{a_\pm}=\frac{i}{\sqrt{2}}L_{1\pm1}. \tag{18}$$

Since the direct product $T_1\times T_1$ in **O** contains E and T_2, the matrices $\mathbf{O}_{E\gamma}$ and $\mathbf{O}_{T_2\gamma}$ can be expressed through the bilinear forms of $\mathbf{O}_{T_1\gamma}$ using the Clebsch–Gordan decomposition,

$$\mathbf{O}_{\Gamma\gamma}=K_\Gamma\sum_{\gamma_1\gamma_2}\mathbf{O}_{T_1\gamma_1}\mathbf{O}_{T_1\gamma_2}\langle T_1\gamma_1T_1\gamma_2|\Gamma\gamma\rangle, \tag{19}$$

where K_Γ are the numerical coefficients. In this way all $\mathbf{O}_{\Gamma\gamma}$ matrices in the Hamiltonian (9) can be expressed in terms of the bilinear forms $L_{1q_1}L_{1q_2}$. Taking into account that $L_{1q}\equiv T_{1q}(L)$ is the first rank irreducible tensor of spherical group R_3, one can express all one-site operators, $\mathbf{O}_{\Gamma\gamma}$, through the irreducible tensors $T_{kq}(L)$ of ranks $k=0,1,2$,

$$L_{1q_1}L_{1q_2}=\sum_{kq}T_{kq}(L)\langle kq|1q_11q_2\rangle, \tag{20}$$

where $\langle kq|1q_11q_2\rangle$ are the Wigner coefficients.

The last step is to express the direct products $\mathbf{O}^A_{\Gamma\gamma}\mathbf{O}^B_{\Gamma'\gamma'}$ (two site operators) involved in the Hamiltonian (9) through the irreducible tensor products $\{T^A_{k_A}(L_A)\otimes T^B_{k_B}(L_B)\}_{kq}$. This can be done using the Clebsch–Gordon decomposition once more,

$$T^A_{k_Aq_A}(L_A)T^B_{k_Bq_B}(L_B)=\sum_{k=|k_A-k_B|}^{k_A+k_B}\{T^A_{k_A}(L_A)\otimes T^B_{k_B}(L_B)\}_{kq}\langle kq|k_Aq_Ak_Bq_B\rangle. \tag{21}$$

For instance, the product $\mathbf{O}^A_{x_0}\mathbf{O}^B_{x_0}$ can be expressed through the tensor products of ranks $k=0$, 2, and 4 and $q=0$,

$$\mathbf{O}^A_{x_0}\mathbf{O}^B_{x_0}=\frac{1}{\sqrt{5}}\{T^A_2\otimes T^B_2\}_{00}-\frac{2}{\sqrt{14}}\{T^A_2\otimes T^B_2\}_{20}+\frac{6}{\sqrt{70}}\{T^A_2\otimes T^B_2\}_{40}. \tag{22}$$

The Hamiltonian expressed in terms of the irreducible tensor operators acts within the basis set $|L_AL_BS_AS_B,SM_SLM_L\rangle\equiv|SM_S,LM_L\rangle$ with fictious $L_A=L_B=1$ and $L=0,1,2$ (Russell–Saunders coupling scheme). This provides an alternative way to calculate the energy levels applying the powerful technique of the irreducible tensor operators of R_3, and extend also the effective Hamiltonian approach to the polynuclear clusters. All related interactions (low-symmetry crystal fields, spin–orbit coupling, Zeeman interactions) are also incorporated in the unified computational scheme.[23]

The results obtained in this way allows us to show in Fig. 4, along with the irreducible representations of D_{3h}, the corresponding $|SM_S,LM_L\rangle\equiv|S;LM_L\rangle$ labels related to the pseudoangular momentum representation. Using this labeling we can make some qualitative conclusion about the magnetic anisotropy of the system.

Let us start with the pseudospherical case (i). The ground level comprises two terms $^3A_2'$ and $^3E'$ that can be associated with $|1;10\rangle$ and $|1;2\pm1\rangle$ functions. The spin part of the exchange Hamiltonian is evidently isotropic, so the anisotropy comes from the orbital contributions. One can see that $|1;2\pm1\rangle$ states give strong orbital contribution to $\chi_\parallel$, meanwhile the matrix elements of L_x and L_y disappear within the ground manifold ($L=1$ for $^3A_2'$ and $L=2$ for $^3E'$). Inspecting in the same way all $|S;LM_L\rangle$ labels one can see that the operator L_z has nonvanishing matrix elements within all levels with $M_L\neq0(L=1,2)$. On the contrary, the matrix elements of L_x and L_y vanish within each exactly and accidentally degenerate level in Fig. 4. The matrix elements of these operators vanish also within the basis belonging to six low-lying levels. The nonvanishing matrix elements link only the low-lying states with the highest group of states. For these reasons the perpendicular component of the orbital part of the magnetic susceptibility appears as the second-order effect and hence one can expect that $\chi_\parallel>\chi_\perp$, so the magnetic anisotropy defined as $\Delta\chi=\chi_\parallel-\chi_\perp$ proves to be positive.

Our conclusion that the exchange interaction produces a strong magnetic anisotropy in a face-shared bioctahedral molecule under the condition $t'=0$ [case (i)] is in striking contradiction with the statement of Drillon and Georges.[8] In fact, in their model, the exchange anisotropy does not exist providing $t'=0$; it can appear only as a minor effect due to the contributions of the crossing transfer terms $\propto tt'$ and t'^2. The origin of this discrepancy will be discussed later on.

Finally, we would like to underline that each level in case (i) is $(2M_L+1)$-fold degenerate (like in the spherically symmetric system) but does not correspond to a definite value of $L=M_{L\,\max}$ (for example, $L=1$ and $L=2$ in the ground state with $M_L=-1,0,1$) as indicated in Fig. 4. For this reason, we refer to this case as pseudospherical (but not spherical) limit. Indeed, from the point of view of magnetic anisotropy so far discussed this case should be referred to as completely anisotropic. It is to be noted that the pseudospherical limit occurs under the ''spherical'' condition $t_a=t_e$ for the transfer integrals.

Let us consider now the spherical case (ii). The energy levels are the same as in the previous case (Fig. 3) but the

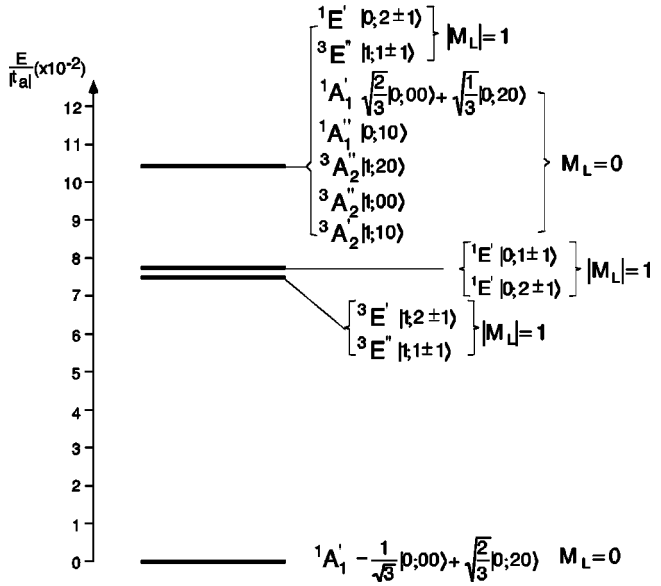

FIG. 5. Energy pattern of the face-shared $^2T_2-^2T_2$ system in the axial limit.

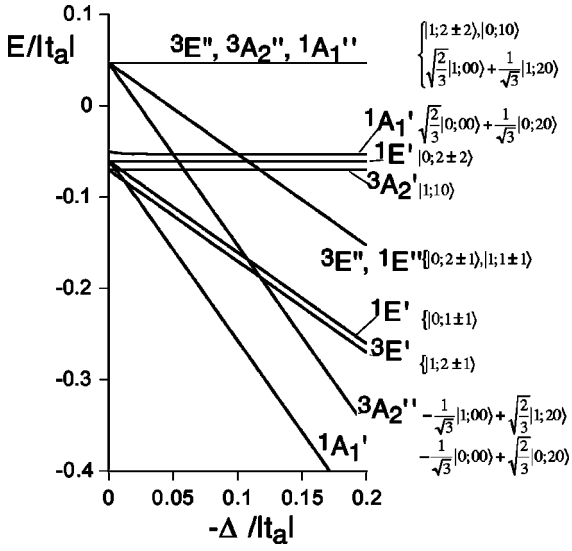

FIG. 6. Influence of the trigonal field ($\Delta<0$) on the energy pattern in the pseudospherical limit.

wave functions are different (see labels in the left part of Fig. 4). The general feature of this energy pattern is that each level can be associated to one or several atomic terms *SL* as shown in Fig. 4. In fact, the ground state containing accidentally degenerate levels $^3A_2'(|1;10\rangle)$, $^3E''(|1;1,\pm1\rangle)$ can be regarded as an atomic term with $L=1$ and $S=1$, the first excited state possesses $L=2$ and $S=0$, etc. This shows that, as distinguished from the previous case, the system in the limit $t_a/t_e=-1$ is magnetically isotropic. Therefore, this case can be referred to as true spherical limit.

The last case we consider here is the axial limit ($t_e=0$). In this case the ground state is the orbital and spin singlet $^1A_1'$ [that corresponds to the wave-function $-(1/\sqrt{3})|0;00\rangle+\sqrt{\frac{2}{3}}|0;20\rangle$ in pseudoangular momentum representation (Fig. 5)]. The first excited group of levels consists of two closely spaced sublevels. One of them (lower) comprises spin triplets $^3E'$, $^3E''$, and another spin singlets $^1E'$, $^1E''$. Finally, the highest level comprises both spin triplets and spin singlets. A similar energy diagram was obtained by Leuenberger and Güdel,[4] but in their energy scheme the first excited level was not split. This is a result of ignoring the differences in energies of charge-transfer states. Since $M_L=0$ and $S=0$ in the ground state, $\chi_\parallel=0$ in the low temperature limit. At the same time the perpendicular magnetic susceptibility appears as a second order effect (temperature independent Van Vleck paramagnetism) due to the mixing of the ground state with the excited states $|0;2\pm1\rangle(^1E'')$ through the orbital part of Zeeman interaction. The anisotropy $\Delta\chi$ proves to be negative, i.e., it has the reverse sign with respect to the pseudospherical case.

This conclusion about negative magnetic anisotropy is valid also for the range of t_e/t_a (Fig. 3) in which the ground term is $^1A_1'$ (superposition of $|0;00\rangle$ and $|0;20\rangle$). When $^3E''$ ($t_e/t_a<-0.9$) or $^3E'$ ($t_e/t_a>0.9$) are the ground terms ($M_L=\pm1$), $\Delta\chi$ is positive. In all cases (with the exception of the true spherical limit $t_e/t_a=-1$) the magnetic anisotropy is axial ($|M_L|$ is a good quantum number) and $\Delta\chi$ depends on the ratio t_e/t_a. In this view, it should be noted that we have used the term ''axial'' for the case (iii) only to indicate axial interrelation between t_e and t_a. It should be noted also that in all cases the states of the system are the eigenvectors of L_z so that no second order Zeeman effect is possible in the parallel field.

VI. TRIGONAL CRYSTAL FIELD

For the realistic description of the magnetic properties of the $[Ti_2Cl_9]^{-3}$ binuclear unit one should take into account along with the exchange interaction also the contribution of the trigonal crystal fields acting on each metal site and spin–orbit coupling. Let us consider first the energy pattern resulting from the combined effect of exchange interaction and local trigonal crystal field (site symmetry C_{3V}). We define the trigonal crystal field $\mathbf{V}_{\text{trig}}=\mathbf{V}^A_{\text{trig}}+\mathbf{V}^B_{\text{trig}}$ introducing the energy separation between the orbitals $x_0^{A(B)}$ (A_1 in C_{3V}) and $x_\pm^{A(B)}(E)$,

$$\langle x_0^{A(B)}|\mathbf{V}^{A(B)}_{\text{trig}}|x_0^{A(B)}\rangle=\Delta,\langle x_\pm^{A(B)}|\mathbf{V}^{A(B)}_{\text{trig}}|x_\pm^{A(B)}\rangle=0. \qquad (23)$$

The trigonal crystal field mixes the repeated terms $2\,^3A_2''$, $2\,^3E''$, $2\,^1A_1'$ and $2\,^1E'$ (see Appendix D).

The correlation diagram in Fig. 6 illustrates how the pattern of the energy levels formed by the exchange interaction in $^2T_2-^2T_2$-pair in the pseudospherical limit is modified under the influence of the trigonal crystal field providing $\Delta<0$ (orbital singlet $^2A_1$ in the ground state of each ion). As one can see from Fig. 6 the trigonal field partially removes the accidental degeneracy of the exchange multiplets contributing antiferromagnetically to the low-lying group of levels. The increase of the absolute value of the trigonal field parameter $|\Delta|$ leads to the crossing of the spin levels $^1A_1'$ and $^3E'$ so that the system becomes antiferromagnetic, even for a very weak trigonal field. In the limit of strong trigonal field, the low-lying group of levels proves to be well isolated and consists of the orbitally nondegenerate spin singlet $^1A_1'$ (ground) and the spin triplet $^3A_2''$; the energy separation be-

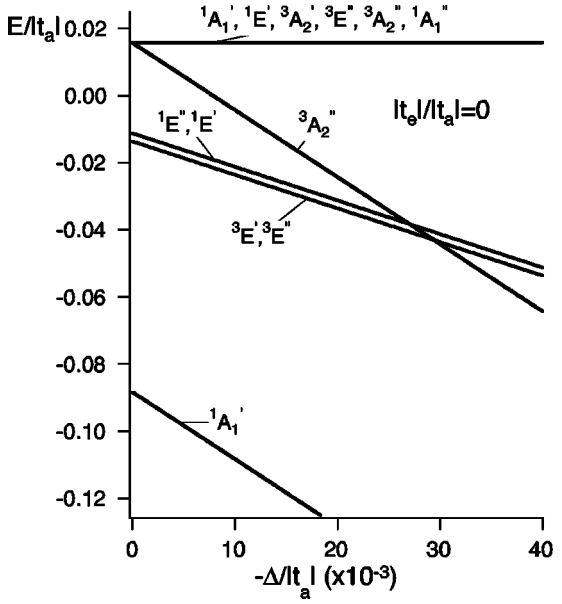

FIG. 7. Influence of the trigonal field ($\Delta<0$) on the energy pattern in the axial limit.

tween them is found to be $\varepsilon({}^3A_2'')-\varepsilon({}^1A_1')=-(J_1+J_3)$. This pair of levels can be described by the isotropic HDVV Hamiltonian $-2J_{\text{eff}}\mathbf{S}_A\mathbf{S}_B$ with $J_{\text{eff}}=\frac{1}{2}(J_1+J_3)$. The exchange interaction proves to be antiferromagnetic ($J_{\text{eff}}<0$) and this is just what one could expect according to the Anderson's theory[24] and Goodenough–Kanamori rules[25] for a pair of ions possessing half-filled nondegenerate orbitals x_0^A, x_0^B well separated from the excited states. The energy levels can be conventionally subdivided into three groups depending on their sensitivity to the trigonal field. Singlet–triplet pair ${}^1A_1'$, ${}^3A_2''$ can be assigned to $a\times a$-group, orbital doublets ${}^1E''$, ${}^1E'$, ${}^3E'$, ${}^3E''$ belong to $a\times e$, and the rest arises from the $e\times e$-group.

Concerning the influence of trigonal field on the magnetic behavior two points should be mentioned. First, the trigonal field should strongly reduce the magnetic susceptibility because of the stabilization of the state ${}^1A_1'$ that carries neither spin nor orbital magnetic moment. Second, the trigonal field tends to change the sign of the anisotropy. At the low temperatures $\chi_{\parallel}$ tends to zero, meanwhile $\chi_{\perp}$ tends to the nonzero value due to a second order Zeeman effect. In fact, inspecting the $S;LM_L$-labels in Fig. 6 one can see that the ground state ${}^1A_1'$ $(-(1/\sqrt{3})|0;00\rangle+\sqrt{\frac{2}{3}}|0;20\rangle)$ can be mixed through $L_{\perp}$ with the state ${}^1E''(|0;2\pm1\rangle)$, whereas L_z cannot mix the ground state with the excited states. With the further increase of $|\Delta|$ the second-order effect decreases and the system becomes more isotropic.

Providing $\Delta>0$ (the orbital doublet ${}^2E$ is the ground state for each ion) the ground state of the system is the spin triplet ${}^3A_2'$ independently of the trigonal field Δ, i.e., the face-shared ${}^2T_2-{}^2T_2$ pair in this case is always ferromagnetic. In the limit of strong trigonal field the pattern of low-lying levels comprises three levels ${}^3A_2'$, ${}^1E'$, ${}^1A_1'$ and accidentally degenerate level ${}^3E''$, ${}^3A_2''$, ${}^1A_1''$. These four low-lying levels are obviously the solutions of the ${}^2E(x_{\pm})-{}^2E(x_{\pm})$ exchange problem.

In the axial case the trigonal field $\Delta<0$ does not change the ground state ${}^1A_1'$ leading to its additional stabilization (Fig. 7). The spin triplet ${}^3A_2''$ arising from the highest group of levels is stabilized in the same way, so in the strong crystal field limit singlet–triplet pair proves to be well isolated. Therefore, in the limit of strong negative crystal field the axial and pseudospherical cases are similar. At the same time the situation for $\Delta>0$ in axial case is quite different from the pseudospherical one because the ground level now is accidentally degenerate $({}^1A_1',{}^1E',{}^3A_2',{}^3E'',{}^3A_2'',{}^1A_1'')$. This is obviously due to the fact that only t_e transfer is responsible for the splitting of the $e\times e$ group.

VII. SPIN–ORBIT AND ZEEMAN INTERACTIONS

The adequate description of the magnetic properties, and particularly the magnetic anisotropy demands to take into account the spin–orbit interaction. This interaction for the $A-B$ pair can be described by the operator,

$$\begin{aligned}\mathbf{H}_{\text{SO}}&=k\lambda(\mathbf{L}_A\mathbf{S}_A+\mathbf{L}_B\mathbf{S}_B')\\&=k\lambda(L_{10}^AS_{10}^A-L_{11}^AS_{1-1}^A-L_{1-1}^AS_{11}^A+L_{10}^BS_{10}'^B\\&\quad-L_{11}^BS_{1-1}'^B-L_{1-1}^BS_{11}'^B),\end{aligned}\tag{24}$$

where k is the orbital reduction factor arising from the effect of covalence and λ is the spin–orbit parameter for the free ion. In Eq. (24) the orbital angular momentum operators $L_{1q}^{A(B)}$ [as well as the orbital matrices $\mathbf{O}_{\Gamma\gamma}^{A(B)}$ in the effective exchange Hamiltonian] are defined in the local trigonal coordinate systems [Figs. 1(b) and 1(c)]. The operator $\mathbf{S}_A$ is defined in the same way as in the exchange Hamiltonian (9), i.e., in the molecular coordinate system coinciding with the local trigonal system for the site A. On the contrary, $\mathbf{S}_B'$ relates to the local trigonal system of the site B, that differs from the molecular one, the directions of X and Y-axes being opposite. Using the relationships $S_{10}'^B=S_{10}^B, S_{1-1}'^B=-S_{1-1}^B, S_{11}'^B=-S_{11}^B$ one can represent the operator $\mathbf{H}_{\text{SO}}$ as follows:

$$\begin{aligned}\mathbf{H}_{\text{SO}}&=k\lambda(L_{10}^AS_{10}^A-L_{11}^AS_{1-1}^A-L_{1-1}^AS_{11}^A+L_{10}^BS_{10}^B\\&\quad+L_{11}^BS_{1-1}^B+L_{1-1}^BS_{11}^B).\end{aligned}\tag{25}$$

Now the orbital operators are defined in the local coordinate systems and the spin operators are defined in the molecular system just as in the effective exchange Hamiltonian (9).

The nonvanishing matrix elements of the L_{1q}^i $(i=A,B)$ operators in the one-center trigonal basis are the following:

$$\begin{aligned}&\langle x_{\pm}^i|L_{10}^i|x_{\pm}^i\rangle=\mp1,\langle x_0^i|L_{1\pm1}^i|x_{\mp}^i\rangle\\&\qquad=\pm1,\langle x_{\pm}^i|L_{1\pm1}^i|x_0^i\rangle=\pm1.\end{aligned}\tag{26}$$

The matrix of the spin–orbit interaction has been built using Eq. (26) and taking as a basis the set of symmetry adapted wave functions (Table II).

Finally, one should add to the total Hamiltonian of the pair the Zeeman term $\mathbf{H}_Z$. The orbital part of $\mathbf{H}_Z$ can be written as follows:

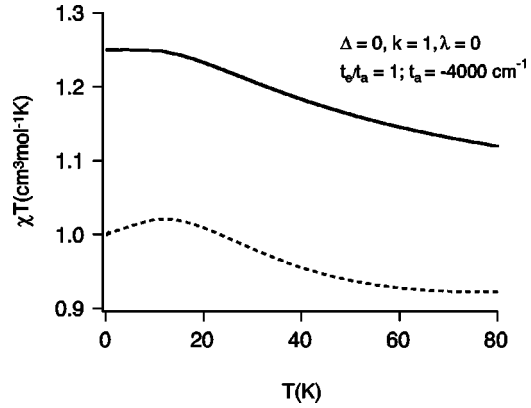

FIG. 8. χT vs T in the pseudospherical limit. Here and in the following figures $\chi_{\parallel}$ is shown by solid lines and $\chi_{\perp}$ by dashed lines.

$$
\begin{aligned}
&k\beta(\mathbf{L}_A\mathbf{H}+\mathbf{L}_B\mathbf{H}') \\
&\quad = k\beta(L^A_{10}H_{10}-L^A_{11}H_{1-1}-L^A_{1-1}H_{11}+L^B_{10}H'_{10} \\
&\qquad -L^B_{11}H'_{1-1}-L^B_{1-1}H'_{11}) \qquad (27)\\
&\quad = k\beta[(L^A_{10}+L^B_{10})H_{10}+(L^B_{11}-L^A_{11})H_{1-1} \\
&\qquad +(L^B_{1-1}-L^A_{1-1})H_{11}],
\end{aligned}
$$

where $\mathbf{L}_A$ and $\mathbf{L}_B$ are related to the local coordinate systems, $\mathbf{H}$ is defined in the molecular system, and $\mathbf{H}'$ relates to the local system B. In the spin part of $\mathbf{H}_Z$ both local spin operators are defined in the molecular coordinate system and thus they can be coupled to give total spin S,

$$
\begin{aligned}
\beta g_e(\mathbf{S}_A+\mathbf{S}_B)\mathbf{H} &= \beta g_e \mathbf{S}\mathbf{H} \\
&= \beta g_e(S_{10}H_{10}-S_{11}H_{1-1}-S_{1-1}H_{1+1}). \qquad (28)
\end{aligned}
$$

Now spin–orbit and Zeeman interactions are represented in the same coordinate frames as the effective exchange Hamiltonian (9).

VIII. MAGNETIC MANIFESTATIONS OF THE MAIN INTERACTIONS

In the discussion of the magnetic properties we will fix Dq and Racah parameters taking for the Racah parameters their values for the free-ion (see Sec. VII). The results will be discussed considering the sample calculations performed at $t_a=-4000\ \mathrm{cm}^{-1}$ (this is within the Anderson's estimation of transfer parameter[24]), $k=1$ and some selected values of t_e/t_a and Δ. We will consider especially the role of spin–orbit coupling, so the results will be presented for two cases: $\lambda=0$ and $\lambda=155\ \mathrm{cm}^{-1}$ (free Ti^{+3}-ion).[9] This discussion will allow us to reveal the role of different relevant parameters before fitting the experimental data.

A. The role of the ratio t_e/t_a

Figure 8 shows the χT vs T dependence for the pseudospherical limit ($t_e/t_a=1$) provided that $\lambda=0$ and $\Delta=0$. One can observe that the magnetic susceptibility is anisotropic with positive anisotropy. The low-temperature limit of $\chi_{\perp}T$ shows pure spin ($S=1$) value, meanwhile $\chi_{\parallel}T|_{T\to 0}=1.25$ exhibits strong orbital contribution. The reason for this behavior was qualitatively explained above with the use of pseudoangular momentum representation. One can note also that $\chi_{\parallel}T$ decreases monotonically with the increase of temperature, meanwhile $\chi_{\perp}T$ passes through the maximum at $T=15\ \mathrm{K}$.

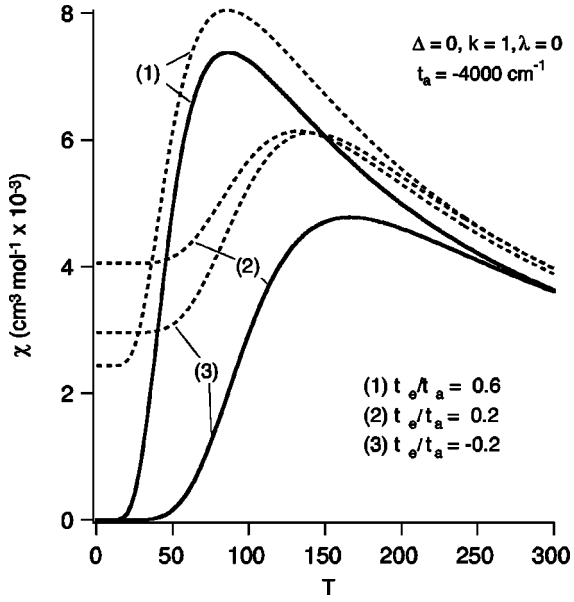

FIG. 9. Influence of the ratio t_e/t_a on the magnetic susceptibility.

Figure 9 demonstrates how the magnetic anisotropy depends on the ratio t_e/t_a in the region where the ground state is the orbital and spin singlet ${}^1A_1'$ (Fig. 3). The following main features of χ vs T curves should be noted: (1) the sign of the anisotropy in this region of t_e/t_a is negative, (2) $\chi_{\parallel}$ tends to zero with the decrease of temperature, (3) the anisotropy increases with the decrease of t_e/t_a, (4) $\chi_{\parallel}$ does not depend on the sign of t_e/t_a (compare the cases $t_e/t_a=\pm 0.2$). The first two features have already been explained in the discussion of the axial limit. The features 3 and 4 can be realized considering the correlation diagram in Fig. 3. The ground state ${}^1A_1'$ is a superposition of two $|S;LM_L\rangle$ states: $|0;00\rangle$ and $|0;20\rangle$. The state $|0;20\rangle$ is mixed in a perpendicular field with the state ${}^1E''(|0;2\pm 1\rangle)$. The efficiency of this mixing depends both on the weight of the wave function $|0;20\rangle$ in ${}^1A_1'$-state and on the energy separation between ${}^1A_1'$ and ${}^1E''$. The calculation shows that in the range of t_e/t_a under consideration the contribution of $|0;20\rangle$ in the ground state increases slightly with the decrease of t_e/t_a. At the same time the gap ${}^1A_1'$, ${}^1E''$ decreases, and hence $\chi_{\perp}$ (and $\Delta\chi$) goes up. To realize the fact that $\chi_{\parallel}$ is independent of the sign of t_e/t_a one should take into account that passing from $|t_e/t_a|$ to $-|t_e/t_a|$ we change only four levels: ${}^1E'\leftrightarrow{}^1E''$ and ${}^3E'\leftrightarrow{}^3E''$ and the coefficients in the linear combinations of $|0;00\rangle$ and $|0;20\rangle$ defining two ${}^1A_1'$ terms. Since E' and E'' relate to the same M_L and ${}^1A_1'$ terms do not contribute to the $\chi_{\parallel}$, this changes does not influence $\chi_{\parallel}$.

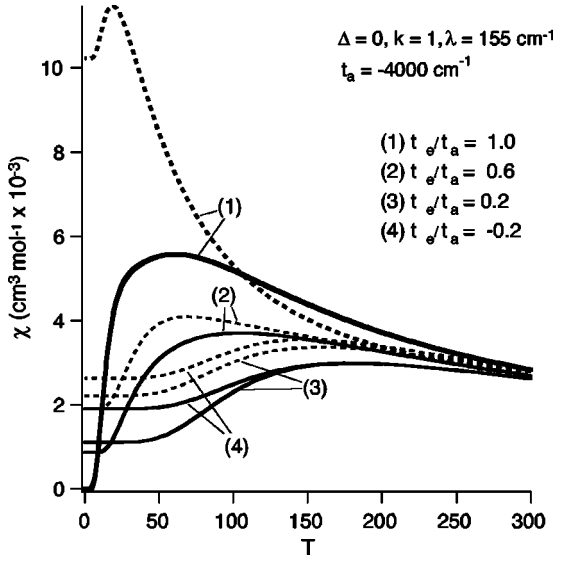

FIG. 10. Influence of the ratio t_e/t_a on $\chi(T)$ in the presence of spin–orbit coupling.

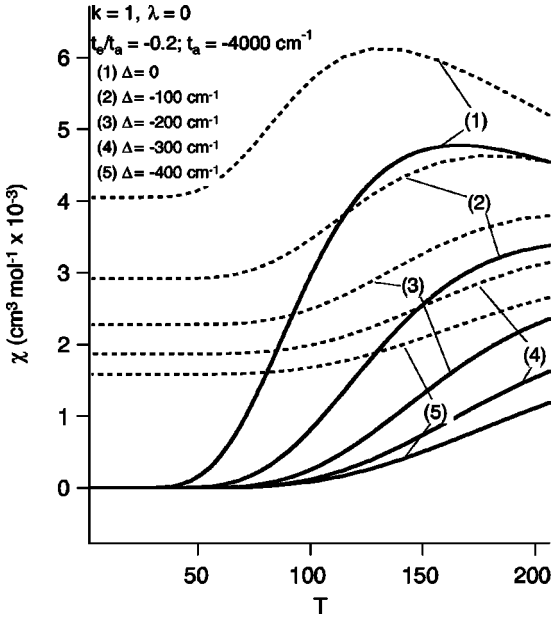

FIG. 12. Influence of the trigonal field on $\chi(T)$.

B. The role of spin–orbit coupling

Spin–orbit interaction in the pseudospherical limit changes dramatically the magnetic behavior (Fig. 10). The main effect is that χ is strongly reduced. Spin–orbit coupling results in the nonmagnetic ground state arising from $^3A_2'$, $^3E'$ manifold, so $\chi_\parallel$ goes to zero at low temperatures and $\chi_\perp$ appears as a second order effect. Therefore as distinguished from the case $\lambda=0$ (Fig. 8) the magnetic anisotropy becomes negative.

The spin–orbit interaction in the intermediate region of t_e/t_a (ground $^1A_1'$) gives rise to the nonvanishing low-temperature limit of $\chi_\parallel$ (Fig. 10) due to spin–orbit mixing with the excited spin triplets carrying orbital magnetic momenta. The low-temperature $\chi_\parallel$ increases when t_e/t_a decreases (mainly as a result of the increase of $^1A_1'$, $^3E'$ gap).

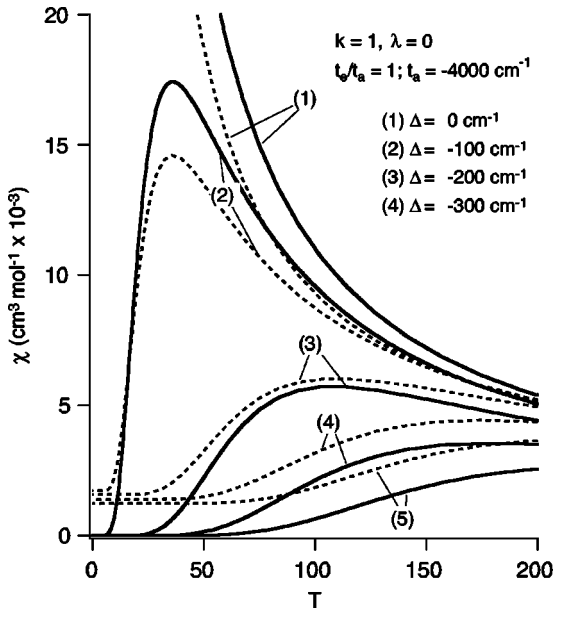

FIG. 11. Influence of the trigonal field on $\chi(T)$ in the pseudospherical limit.

At the same time spin–orbit interaction slightly modifies $\chi_\perp$, so that $\Delta\chi$ remains positive. Due to spin–orbit coupling $\chi_\parallel$ becomes dependent on the sign of t_e/t_a (compare with the case $\lambda=0$, Fig. 9).

C. The influence of trigonal crystal field

Figure 11 clearly shows that trigonal crystal field under the conditions of pseudospherical limit changes the ground state reversing thus the sign of $\Delta\chi$. The anisotropy disappears with the increase of $|\Delta|$ in accordance with the arguments given in Sec. VI. The maximum of χ vs T curve moves to the high-temperature region with simultaneous decrease of the maximum values of χ. One can see that negative trigonal crystal field restores the Heisenberg-type magnetic behavior (Bleaney–Bowers equation)[9] peculiar for a well isolated singlet–triplet spin pair.

In the intermediate region of t_e/t_a (Fig. 12) we observe also the decrease of anisotropy at low temperatures with the increase of $|\Delta|$. The remarkable features of the magnetic behavior of the system in the moderate temperature range should be noted. First, the slope of the increase of $\chi_{\perp,\parallel}(T)$ strongly depends on Δ increasing (decreasing) with the decrease (increase) of $|\Delta|$. This effect is obviously due to the changes in the gap between the ground state and the set of exchange levels contributing to $\chi(T)$ when these levels are thermally populated. Second, the maximum values of $\chi(T)$ depend on Δ similarly. Third, the degree of anisotropy decreases with the increase of T. This important effect appears due to the thermal population of the levels ($|S;1\pm1\rangle$, $|S;2\pm2\rangle$) exhibiting first order orbital Zeeman splitting and contributing thus to $\chi_\parallel$. The low-temperature limits of $\chi_\perp(T)$ and the slope in $\chi(T)$ depend strongly also on the energy gap between $^1A'$ and $^3A_2''$. Finally, it can be noted that in the presence of trigonal crystal field $\chi_\parallel$ (T) remains independent of the sign of t_e/t_a providing $\lambda=0$.

IX. DISCUSSION OF THE MODELS AND MAGNETIC BEHAVIOR OF $[Ti_2Cl_9]^{-3}$

The first study of magnetic and spectroscopic properties of the salts $[M_2X_9]^{-3}$ (X=Br, I) containing first-row transition metal ions were reported more then 30 years ago by Saillant and Wentworth.[5] Later on Briat, Kahn *et al.*[6] performed a detailed magnetic and spectroscopic study on crystalline samples of $Cs_3Ti_2Cl_9$. They observed that the infrared absorption spectra exhibited a broad featureless band located in the region $800-3000\,cm^{-1}$ that cannot be assigned to a single Ti^{3+} ion transition. This band seems to be closely related to the group of levels created by the exchange interaction in a dimer. The magnetic data indicated that the low-temperature magnetic susceptibility is small and strongly anisotropic with $\chi_\perp > \chi_\parallel$. A remarkable feature of the experimental data is that the magnetic anisotropy decreases with the increase of temperature. Both $\chi_\parallel$ and $\chi_\perp$ decrease when the samples cool down and they become temperature independent at $T<100\,K$. These data clearly show that the ground state of the pair is nonmagnetic.

The measurements of the infrared reflectivity from a single crystal of $Cs_3Ti_2Cl_9$ showed the broad signals between $350\,cm^{-1}$ and $950\,cm^{-1}$.[26] Since no vibration transitions could be expected in this energy range these signals are of magnetic origin indicating that the first excited level has an energy of at least $450\,cm^{-1}$. Similar conclusion was made for polycrystalline sample of $Rb_3Ti_2Br_9$ on the basis of the inelastic neutron scattering experiments exhibiting a broad band of magnetic origin between $400\,cm^{-1}$ and $600\,cm^{-1}$.[26]

Briat, Kahn *et al.*[6] employed the theoretical model of Kahn[27] involving trigonal crystal field stabilizing the local orbital singlets, isotropic exchange, and spin–orbit coupling. An attempt was also made to take into account the degeneracy of the Ti^{+3} ions by introducing orbit-orbit interaction of the form $-K\mathbf{L}_A\mathbf{L}_B$. Although this model does not take into account all relevant terms involved in the Hamiltonian of T_2-T_2-interaction it provides an important indication on the range of parameters that are responsible for the $\chi(T)$ dependence. Particularly the gap between $^1A'$ and $^3A_2''$ is estimated to be $630\,cm^{-1}$, this value provides a satisfactory explanation of the slope of $\chi(T)$ observed at $T>100\,K$.

The concept of the effective kinetic exchange Hamiltonian for orbitally degenerate ions was developed by Drillon and Georges.[3] For the first time they applied their approach to the face-shared D_{3h} system and analyzed the magnetic behavior of $[Ti_2Cl_9]^{-3}$ taking into account also spin–orbit interaction and the trigonal component of the crystal field.[8] The effective Hamiltonian obtained by Drillon and Georges[8] is expressed in terms of the orbital operators $\mathbf{L}_{A(B)}$ acting in T_2 and spin operators $\mathbf{S}_{A(B)}$. In the fit procedure Drillon and Georges neglected crossing transfer integrals $(t'=0)$, that corresponds to the relationship $t_a=t_e$ (pseudospherical limit in our classification). In this case the effective Hamiltonian contains the scalar products: $\mathbf{L}_A\mathbf{L}_B$, $(\mathbf{L}_A\mathbf{L}_B)^2$, $\mathbf{L}_A\mathbf{L}_B\mathbf{S}_A\mathbf{S}_B$, $(\mathbf{L}_A\mathbf{L}_B)^2\mathbf{S}_A\mathbf{S}_B$, and $\mathbf{S}_A\mathbf{S}_B$. For this reason, this Hamiltonian was regarded as isotropic, and LS labels $(L=0,1,2)$ for the eigenvalues have been used. At the same time according to the authors[8] the inclusion of the crossing transfer terms $(t'\neq 0)$ leads to the magnetic anisotropy due to the appearance of the contributions like $L^A_{10}L^B_{10}$, etc. Since the crossing transfer terms were regarded as small corrections these authors[8] came to the conclusion that the exchange anisotropy is a minor effect and the main reason for the observed anisotropy of $[Ti_2Cl_9]^{-3}$ is the combined effect of trigonal crystal field and spin–orbit coupling, i.e., local (one-site) anisotropy. This conclusion is in clear contradiction with our results. In fact, we have shown that the exchange Hamiltonian is fully anisotropic even providing $t'=0$ and $\Delta\chi$ is negative $(\chi_\perp<\chi_\parallel)$. The inclusion of crossing terms is shown to change the sign of anisotropy. In this respect, it should be emphasized that the crossing terms themselves cannot be considered as a source of the exchange anisotropy.

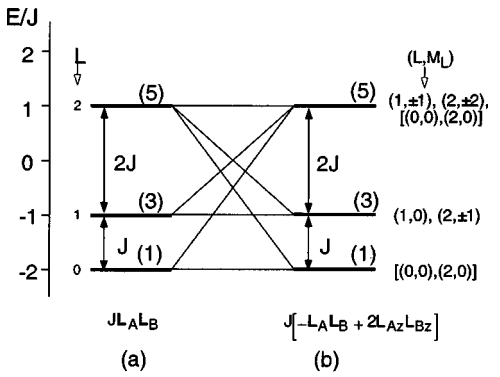

FIG. 13. Correlation diagram for the isotropic (a) and anisotropic (b) operators of orbital interactions. [(0, 0), (2, 0)] is the notation for mixed states with $L=0$ and $L=2$.

The origin of the descrepancy in the understanding of the anisotropic properties of the exchange Hamiltonian in the cited paper[8] and in the present one can be clarified by considering a selected orbital contribution to $\mathbf{H}$, for instance, the term

$$\mathbf{H}' = -2t_a t_e F^{(0)}_{T_1}(-\mathbf{O}^A_{a_+}\mathbf{O}^B_{a_-} - \mathbf{O}^A_{a_-}\mathbf{O}^B_{a_+} + \mathbf{O}^A_{a_0}\mathbf{O}^B_{a_0}). \quad (29)$$

Passing to the orbital angular momenta operators [Eq. (18)] one can present this term as

$$\mathbf{H}' = J(L^A_z L^B_z + L^A_x L^B_x + L^A_y L^B_y), \quad (30)$$

where $J=t_a t_e F^{(0)}_{T_1}$. The operator part in Eq. (30) looks like scalar product $\mathbf{L}_A\mathbf{L}_B$ but in fact it is not a scalar product, because $\mathbf{L}_A$ and $\mathbf{L}_B$ are defined in different trigonal frames A and B. Transforming $\mathbf{L}_B$ to the molecular frame (A) we arrive at the anisotropic operator,

$$\mathbf{H}' = J(-\mathbf{L}_A\mathbf{L}_B + 2L^A_z L^B_z). \quad (31)$$

Figure 13 represents the diagram correlating the eigenvalues of the anisotropic operator $\mathbf{H}'$ (b) (good quantum number $|M_L|$) with those of scalar operator $J\mathbf{L}_A\mathbf{L}_B$ (a) (good quantum number L, with $L=0,1,2$). It is to be noted parenthetically that in this special case the anisotropic operator

gives the same scheme of the energy levels, obeying the Lande's rule, as the isotropic operator does.

The above consideration shows that the conclusion made by Drillon and Georges[8] about the isotropic character of the exchange Hamiltonian and misleading labeling of the eigenstates could be the result of overlooking of the assignment of the operators $\mathbf{L}_A$ and $\mathbf{L}_B$ to different frames. In this view our conclusion about the role of crossing transfer terms also differs from their conclusion.

Inferring this discussion we would like to mention the critical comments of Ceulemans *et al.*[10] addressed to the study of Drillon and Georges. According to the statement of Ceulemans *et al.*, the isotropy of the exchange Hamiltonian in the approach of Drillon and George is the consequence of ignoring the difference (in sign and magnitude) between hopping integrals t_a and t_e. On the contrary, as we have proven in Sec. V, the model $t_a = t_e$ corresponds to the pseudospherical (but not true spherical) limit that is absolutely magnetically anisotropic. In view of this result, the above mentioned comment of Ceulemans *et al.* seems to be erroneous. On the other hand, as we have just demonstrated, the artificial isotropy in Ref. 8 proved to be a result of the misunderstanding in treating of the coordinate systems in the D_{3h} case and the correct application of the model suggested by Drillon and Georges[8] would lead to the anisotropic exchange Hamiltonian.

Leuenberger and Güdel[4] proposed the approach that is similar to that of Drillon and Georges in its background but different in mathematical procedure and in the model of transfer pathways. They suggested a new model implying strong difference between two transfer integrals ($t_a^2 \gg t_e^2$). This is quite different from the assumption made in Ref. 8, where the pseudospherical limit was considered. At the same time, as distinguished from Ref. 8, the model of Leuenberger and Güdel ignores the differences in the energies of spin singlets and spin triplets in the reduced states, that is important for the adequate description of the kinetic exchange splittings.

Ceulemans *et al.*[10] constructed a second order perturbational Hamiltonian and presented a series of *ab initio* calculations for $[Ti_2Cl_9]^{-3}$. These calculations confirmed the conclusion of Ref. 4 about strong differences in the magnitudes of t_a and t_e. Moreover, these calculations clearly demonstrated that t_a and t_e should have opposite signs.

In order to restrict the number of the adjustable parameters in fitting of the experimental data we will use the ratio of two transfer integrals t_a and t_e extracted from the *ab initio* calculations of Ceulemans and co-workers.[10] They roughly estimated this ratio as $t_a/t_e \approx -6.5$ (-7 in Refs. 11 and 12), that corresponds to $t'/t = 1.67$.

In the best fit procedure we use the same values for the crystal field and Racah parameters as in Sec. VII, $\lambda = 155\,\mathrm{cm}^{-1}$, and vary t_a, Δ, and k. Figure 14 displays the experimental temperature dependencies of $\chi_\parallel$ and $\chi_\perp$ for $Cs_3Ti_2Cl_9$ obtained by Briat, Kahn *et al.*[6] and the theoretical curves. The best fit is achieved for $t_a = -5208\,\mathrm{cm}^{-1}$, $\Delta = -320\,\mathrm{cm}^{-1}$, and $k = 0.71$. One can see that the theoretical curve for $\chi_\perp$ is in an excellent agreement with the experimental data in the low-temperature region (below 170 K). The calculated $\chi_\parallel$ at low temperature is in satisfactory agreement with the experimental values. It is remarkable also that the theory well reproduces the slopes of $\chi_\parallel$ and $\chi_\perp$. Another important feature of the magnetic behavior of $Cs_3Ti_2Cl_9$ is the temperature dependence of the magnetic anisotropy. Figure 14 (insert) shows that in a good agreement with the experimental data $\Delta\chi_{\mathrm{theor}}$ remains constant below 100 K and decreases with the increase of T at $T > 150$ K. The calculated values of $\Delta\chi$ ($590\,\mathrm{cm}^3\,\mathrm{mol}^{-1}$ at 100 K and $410\,\mathrm{cm}^3\,\mathrm{mol}^{-1}$ at 320 K) are close to the experimental ones (540 and $410\,\mathrm{cm}^3\,\mathrm{mol}^{-1}$, respectively).

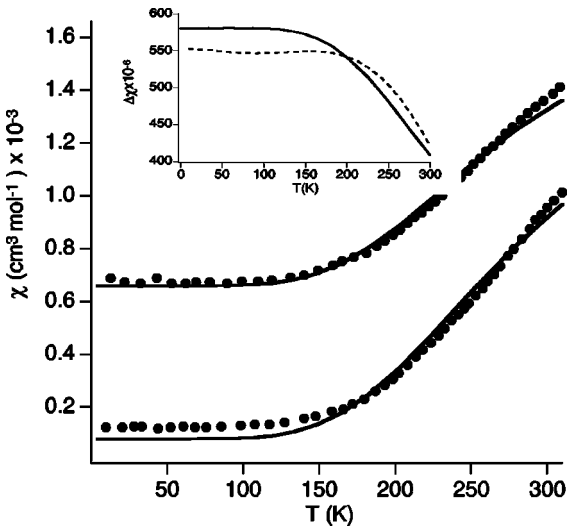

FIG. 14. Magnetic behavior of the $[Ti_2Cl_9]^{-3}$ unit, comparison with the theoretical curve (solid line) calculated at $t_e/t_a = -0.154$, $t_a = -5208\,\mathrm{cm}^{-1}$, $\Delta = -320\,\mathrm{cm}^{-1}$, $\lambda = 155\,\mathrm{cm}^{-1}$, and $k = 0.71$. Insert: Temperature dependence of the degree of anisotropy, comparison with the theoretical curve (solid line).

Figure 15 shows the energy scheme (without spin–orbit coupling) calculated with the set of best fit parameters. The ground state $^1A_1'$, the first excited state $^3A_2''$ is separated by $706\,\mathrm{cm}^{-1}$ from the ground one ($a\times a$-group). The next four orbital doublets ($^3E''$, $^1E''$, $^3E'$, and $^1E'$) fill the gap $135\,\mathrm{cm}^{-1}$ ($a\times e$-manifold). This group of levels is close to $^3A_2''$. Finally, $e\times e$-group of levels forms a narrow band at about $1340\,\mathrm{cm}^{-1}$. One remark should be made concerning the Coulomb repulsion. Analyzing the joint action of this repulsion and trigonal field (Appendix D) one can see that the main effect of the Coulomb repulsion is to redetermine the gaps between $a\times a$, $a\times e$, and $e\times e$ levels. Particularly, the gap between $a\times a$ and $a\times e$ becomes $-\Delta - U_0 + U_1$. Since the $e\times e$ levels are not thermally populated at $T < 300$ K they do not contribute to $\chi(T)$, so the information about these levels cannot be extracted from the best fit. In this view, the parameter $-\Delta$ could be regarded as an effective crystal field parameter associated with the $(a\times e) - (a\times a)$ gap reduced by the Coulomb repulsion due to a predominant destabilization effect on $a\times a$ levels.

Several versions of *ab initio* calculations presented by Ceulemans *et al.*[10] give quite different results for the $^1A_1'$, $^3A_2''$ gap and relative positions of $a\times a$, $a\times e$, and $e\times e$ groups. For the description of the magnetic properties in Ref. 12, the results of CASPT2(v)C calculations were used. Com-

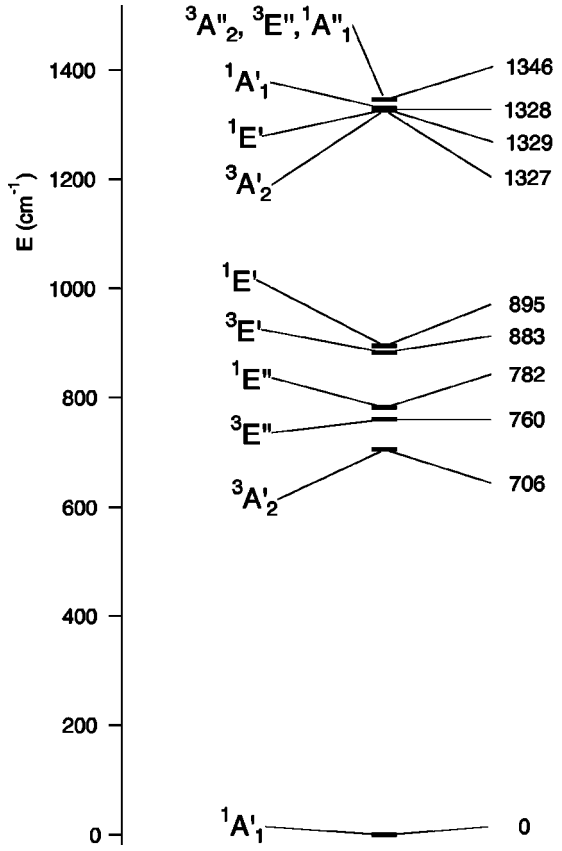

FIG. 15. Energy pattern for the set of best fit parameters.

paring our best fit scheme of levels (Fig. 15) with these results, we can note that our scheme is most close (at least qualitatively) to the result obtained by CASPT2(v)A, mainly in the positions of the levels arising from $a\times a$ and $a\times e$ groups that are responsible for the magnetic behavior below 300 K. Particularly, the $^1A_1'$ $^3A_2''$ gap (718 cm^{-1}) is close to our result. At the same time we have obtained the opposite order of $^3E''$ and $^1E'$ levels originating from $a\times e$. Since the gap $^3E''$, $^1E'$ is small in all *ab initio* calculations as well as in our scheme, the estimation of this gap is probably beyond the accuracy of theoretical predictions.

Finally, one should mention the *ab initio* study of Chen *et al.*[28] The $^1A_1'$, $^3A_2''$ gap reported in their paper (320 cm^{-1}) is too small to account for the experimentally observed slope of $\chi(T)$ at $T>150$ K and the position of the excited levels ($a\times e$-group in the range of 1680–1850 cm^{-1}) is too high to be able to explain the low temperature magnetic anisotropy and its temperature dependence.

Concluding this discussion we would like to make some general comments concerning the effective Hamiltonian. Ceulemans *et al.*[10] constructed a second order kinetic exchange Hamiltonian acting within the ground manifold. This Hamiltonian contains creation (annihilation) operators acting thus on spin–orbitals, i.e., one-electron states. For this reason it cannot be regarded as an effective Hamiltonian to the full extent. On the contrary, our effective Hamiltonian is expressed in terms of many-electron operators acting within the space specified by the total quantum numbers of the constituent ions. From this point of view our Hamiltonian represents a genuine effective Hamiltonian. This can be illustrated using the HDVV spin Hamiltonian and comparing two forms

$$\mathbf{H}=-2\sum_{\alpha\beta} J_{A\alpha,B\beta}\mathbf{S}_{A\alpha}\mathbf{S}_{B\beta}$$

and

$$\mathbf{H}=-2J\mathbf{S}_A\mathbf{S}_B \quad J=(n_An_B)^{-1}\sum_{\alpha\beta} J_{A\alpha B\beta};$$

n_A and n_B are the numbers of magnetic orbitals and $J_{A\alpha B\beta}$ are pairwise exchange parameters. The first one contains explicitly all exchange pathways and one-electron operators, while the second one (true effective Hamiltonian) is expressed in terms of the full spin operators $\mathbf{S}_A$ and $\mathbf{S}_B$ and involves the only many-electron exchange parameter J. Although these two forms of the exchange Hamiltonian are physically equivalent, only the second one can be useful for the parametrization of the experimental data and has an irrefutable advantage as a computational tool.

X. CONCLUDING REMARKS

In this paper we have applied the effective kinetic exchange Hamiltonian deduced in Ref. 1 to the case of the face-shared (D_{3h}) bioctahedral $^2T_2$–$^2T_2$-dimer. The analytical expressions are found for the parameters of the exchange Hamiltonian as a function of two relevant transfer integrals t_a and t_e (or t and t'), cubic crystal field and Racah parameters for the charge-transfer states. Using pseudo-angular momentum representation and irreducible tensor operator technique, we have analyzed the influence of different transfer pathways, trigonal crystal field, and spin–orbit coupling on the magnetic anisotropy of the D_{3h} pair arising from the orbital interactions. We have shown that at some special values of the ratio t_e/t_a the system jumps to some high-symmetric limits in which it could be magnetically fully-symmetric (spherical limit) and completely magnetically axial (pseudospherical limit). In both cases the energy pattern exhibits high degree of accidental degeneracy.

The developed theory well reproduces the magnetic behavior of the binuclear units $[Ti_2Cl_9]^{-3}$ in $Cs_3Ti_2Cl_9$ and particularly the temperature dependence of the degree of the magnetic anisotropy.

ACKNOWLEDGMENTS

Financial support of the MEC (Grant No. PB96-0862-C02-02) and the Generalitat Valenciana (Grant No. GVDOC00-01-02) are acknowledged. B.S.T. thanks the University of Valencia for a visiting professor grant and Generalitat of Valencia for the financial support. The authors are grateful to A. Ceulemans and L. Chibotaru for the preprints of their papers (Refs. 11, 12) and for discussion.

APPENDIX A: ORBITAL MATRICES $O_{\Gamma\gamma}$ IN THE TETRAGONAL T_2-BASIS $\xi\eta\zeta$

$$\mathbf{O}_{A_1}=\begin{array}{c}\begin{matrix}\xi & \eta & \zeta\end{matrix}\\ \begin{pmatrix}1&0&0\\0&1&0\\0&0&1\end{pmatrix}\end{array},\quad \mathbf{O}_{Eu}=\begin{pmatrix}-\frac{1}{2}&0&0\\0&-\frac{1}{2}&0\\0&0&1\end{pmatrix},\quad \mathbf{O}_{Ev}=\begin{pmatrix}\frac{\sqrt{3}}{2}&0&0\\0&-\frac{\sqrt{3}}{2}&0\\0&0&0\end{pmatrix},$$

$$\mathbf{O}_{T_1\alpha}=\begin{pmatrix}0&0&0\\0&0&\frac{1}{\sqrt{2}}\\0&-\frac{1}{\sqrt{2}}&0\end{pmatrix},\quad \mathbf{O}_{T_1\beta}=\begin{pmatrix}0&0&-\frac{1}{\sqrt{2}}\\0&0&0\\\frac{1}{\sqrt{2}}&0&0\end{pmatrix},\quad \mathbf{O}_{T_1\gamma}=\begin{pmatrix}0&\frac{1}{\sqrt{2}}&0\\-\frac{1}{\sqrt{2}}&0&0\\0&0&0\end{pmatrix},$$

$$\mathbf{O}_{T_2\xi}=\begin{pmatrix}0&0&0\\0&0&\frac{1}{\sqrt{2}}\\0&\frac{1}{\sqrt{2}}&0\end{pmatrix},\quad \mathbf{O}_{T_2\eta}=\begin{pmatrix}0&0&\frac{1}{\sqrt{2}}\\0&0&0\\\frac{1}{\sqrt{2}}&0&0\end{pmatrix},\quad \mathbf{O}_{T_2\zeta}=\begin{pmatrix}0&\frac{1}{\sqrt{2}}&0\\\frac{1}{\sqrt{2}}&0&0\\0&0&0\end{pmatrix}.$$

APPENDIX B: ORBITAL MATRICES $O_{\Gamma\gamma}$ IN THE TRIGONAL T_2-BASIS $x_+x_-x_0$

$$\mathbf{O}_{A_1}=\begin{array}{c}\begin{matrix}x_+ & x_- & x_0\end{matrix}\\ \begin{pmatrix}1&0&0\\0&1&0\\0&0&1\end{pmatrix}\end{array},\quad \mathbf{O}_{Eu_+}=\begin{pmatrix}0&0&\frac{1}{\sqrt{2}}\\\frac{1}{\sqrt{2}}&0&0\\0&-\frac{1}{\sqrt{2}}&0\end{pmatrix},\quad \mathbf{O}_{Eu_-}=\begin{pmatrix}0&-\frac{1}{\sqrt{2}}&0\\0&0&\frac{1}{\sqrt{2}}\\-\frac{1}{\sqrt{2}}&0&0\end{pmatrix},$$

$$\mathbf{O}_{T_1a_-}=\begin{pmatrix}0&0&0\\0&0&\frac{i}{\sqrt{2}}\\\frac{i}{\sqrt{2}}&0&0\end{pmatrix},\quad \mathbf{O}_{T_1a_+}=\begin{pmatrix}0&0&-\frac{i}{\sqrt{2}}\\0&0&0\\0&-\frac{i}{\sqrt{2}}&0\end{pmatrix},\quad \mathbf{O}_{T_1a_0}=\begin{pmatrix}\frac{i}{\sqrt{2}}&0&0\\0&-\frac{i}{\sqrt{2}}&0\\0&0&0\end{pmatrix},$$

$$\mathbf{O}_{T_2x_-}=\begin{pmatrix}0&-\frac{\sqrt{2}}{\sqrt{3}}&0\\0&0&-\frac{1}{\sqrt{6}}\\\frac{1}{\sqrt{6}}&0&0\end{pmatrix},\quad \mathbf{O}_{T_2x_+}=\begin{pmatrix}0&0&-\frac{1}{\sqrt{6}}\\\frac{\sqrt{2}}{\sqrt{3}}&0&0\\0&\frac{1}{\sqrt{6}}&0\end{pmatrix},\quad \mathbf{O}_{T_2x_0}=\begin{pmatrix}-\frac{1}{\sqrt{6}}&0&0\\0&-\frac{1}{\sqrt{6}}&0\\0&0&\frac{\sqrt{2}}{\sqrt{3}}\end{pmatrix}.$$

APPENDIX C: THE WAVE FUNCTIONS FOR THE REPEATING $\tilde{S}\tilde{\Gamma}$ TERMS OF d^2 ION IN A CUBIC FIELD

$$|1,{}^3T_1\rangle=\cos\theta|t_2^2,{}^3T_1\rangle-\sin\theta|t_2e,{}^3T_1\rangle,$$

$$|2,{}^3T_1\rangle=\sin\theta|t_2^2,{}^3T_1\rangle+\cos\theta|t_2e,{}^3T_1\rangle,$$

$$|1,{}^1A_1\rangle=\cos\alpha|t_2^2,{}^1A_1\rangle-\sin\alpha|e^2,{}^1A_1\rangle,$$

$$|2,{}^1A_1\rangle=\sin\alpha|t_2^2,{}^1A_1\rangle+\cos\alpha|e^2,{}^1A_1\rangle,$$

$$|1,{}^1E\rangle=\cos\beta|t_2^2,{}^1E\rangle-\sin\beta|e^2,{}^1E\rangle,$$

$$|2,{}^1E\rangle=\sin\beta|t_2^2,{}^1E\rangle+\cos\beta|e^2,{}^1E\rangle,$$

$$|1,{}^1T_2\rangle=\cos\delta|t_2^2,{}^1T_2\rangle-\sin\delta|t_2e,{}^1T_2\rangle,$$

$$|2,{}^1T_2\rangle=\sin\delta|t_2^2,{}^1T_2\rangle+\cos\delta|t_2e,{}^1T_2\rangle,$$

where

$$\tan(2\theta)=\frac{12B}{10Dq+9B},\quad \tan(2\alpha)=\frac{2\sqrt{6}(2B+C)}{20Dq-2B-C},$$

$$\tan(2\beta)=-\frac{4\sqrt{3}B}{20Dq-B},\quad \tan(2\delta)=\frac{4\sqrt{3}B}{10Dq-B}.$$

The expressions of the wave-functions $|t_2^2,\tilde{S}\tilde{\Gamma}\tilde{M}\tilde{\gamma}\rangle$, $|t_2e,\tilde{S}\tilde{\Gamma}\tilde{M}\tilde{\gamma}\rangle$, and $|e^2,\tilde{S}\tilde{\Gamma}\tilde{M}\tilde{\gamma}\rangle$ in terms of Slater determinants are given in Ref. 13 (pp. 53 and 54).

APPENDIX D: EIGENVALUES AND ENERGY MATRICES OF THE EFFECTIVE EXCHANGE HAMILTONIAN [EQ. (9)]: TRIGONAL CRYSTAL FIELD AND INTERSITE COULOMB REPULSION (V_C) ARE ALSO INCLUDED

$$\varepsilon[{}^3A_2'({}^1A_1'')]=U_3+t_a^2\left(\frac{1}{18}F_1+\frac{1}{6}F_2+\frac{1}{54}F_3+\frac{1}{27}F_4\right)+t_e^2\left(\frac{1}{9}F_1-\frac{7}{6}F_2+\frac{1}{27}F_3+\frac{2}{27}F_4\right)-t_e^2F_2\left[S(S+1)-\frac{3}{2}\right],$$

$$\varepsilon[{}^3E'({}^1E'')]=\Delta+U_1+t_a^2\left(\frac{1}{72}F_1-\frac{5}{24}F_2+\frac{1}{54}F_3-\frac{5}{108}F_4\right)+t_e^2\left(\frac{5}{72}F_1-\frac{1}{24}F_2+\frac{1}{27}F_3-\frac{1}{108}F_4\right)+t_at_e\left(\frac{1}{12}F_1-\frac{3}{4}F_2+\frac{1}{6}F_4\right)+\left[-(t_a^2+t_e^2)\left(\frac{1}{12}F_1+\frac{7}{36}F_2+\frac{1}{6}F_4\right)+t_at_e\left(\frac{1}{6}F_1-\frac{11}{18}F_2+\frac{1}{3}F_4\right)\right]\left[S(S+1)-\frac{3}{2}\right],$$

$$\langle[\mathrm{I}]\,{}^3A_2''({}^1A_1')|\mathbf{H}+\mathbf{V}_{\mathrm{trig}}+\mathbf{V}_C|[\mathrm{I}]^3A_2''({}^1A_1')\rangle=\tfrac{2}{3}\Delta+\tfrac{1}{3}(U_0+2U_3)+t_a^2(-\tfrac{1}{18}F_1+\tfrac{1}{6}F_2-\tfrac{1}{27}F_3+\tfrac{1}{27}F_4)+t_e^2(\tfrac{1}{3}F_2-\tfrac{5}{27}F_3+\tfrac{2}{27}F_4)+\tfrac{2}{9}t_at_e(F_1-F_3)+\tfrac{1}{9}[t_a^2(2F_1+F_3)+2t_e^2(F_1+2F_3)-4t_at_e(F_1-F_3)][S(S+1)-\tfrac{3}{2}],$$

$$\langle[\mathrm{II}]\,{}^3A_2''({}^1A_1')|\mathbf{H}+\mathbf{V}_{\mathrm{trig}}+\mathbf{V}_C|[\mathrm{II}]^3A_2''({}^1A_1')\rangle=\tfrac{4}{3}\Delta+\tfrac{1}{3}(2U_0+U_3)+t_a^2(-\tfrac{1}{6}F_1+\tfrac{1}{6}F_2-\tfrac{5}{54}F_3+\tfrac{1}{27}F_4)+t_e^2(\tfrac{1}{18}F_1+\tfrac{1}{3}F_2-\tfrac{2}{27}F_3+\tfrac{2}{27}F_4)-\tfrac{2}{9}t_at_e(F_1-F_3)+\tfrac{1}{9}[2t_a^2(2F_1+F_3)+t_e^2(F_1+2F_3)+4t_at_e(F_1-F_3)][S(S+1)-\tfrac{3}{2}],$$

$$\langle[\mathrm{I}]\,{}^3A_2''({}^1A_1')|\mathbf{H}+\mathbf{V}_{\mathrm{trig}}+\mathbf{V}_C|[\mathrm{II}]\,{}^3A_2''({}^1A_1')\rangle=\frac{2\sqrt{2}}{3}\Delta+\frac{\sqrt{2}}{3}(U_0-U_3)+\frac{\sqrt{2}}{9}[-t_a^2(2F_1+F_3)+t_e^2(F_1+2F_3)+t_at_e(F_1-F_3)][2-S(S+1)],$$

$$\langle[\mathrm{I}]\,{}^3E''({}^1E')|\mathbf{H}+\mathbf{V}_{\mathrm{trig}}+\mathbf{V}_C|[\mathrm{I}]\,{}^3E''({}^1E')\rangle=\tfrac{2}{3}\Delta+\tfrac{1}{3}(2U_1+U_2)+t_a^2(\tfrac{1}{36}F_1-\tfrac{1}{12}F_2+\tfrac{1}{54}F_3-\tfrac{1}{54}F_4)+t_e^2(\tfrac{1}{12}F_1+\tfrac{1}{12}F_2+\tfrac{1}{27}F_3-\tfrac{4}{27}F_4)+\tfrac{1}{18}t_at_e(F_1+9F_2-4F_4)+\tfrac{1}{18}[t_a^2(F_1-3F_2+2F_4)+t_e^2(F_1-3F_2+8F_4)+2t_at_e(-F_1+3F_2+4F_4)][S(S+1)-\tfrac{3}{2}],$$

$$\langle[\mathrm{II}]\,{}^3E''({}^1E')|\mathbf{H}+\mathbf{V}_{\mathrm{trig}}+\mathbf{V}_C|[\mathrm{II}]\,{}^3E''({}^1E')\rangle=\tfrac{1}{3}\Delta+\tfrac{1}{3}(U_1+2U_2)+t_a^2(\tfrac{1}{24}F_1+\tfrac{1}{24}F_2+\tfrac{1}{54}F_3+\tfrac{1}{108}F_4)+t_e^2(-\tfrac{17}{72}F_1+\tfrac{5}{24}F_2+\tfrac{1}{27}F_3+\tfrac{5}{108}F_4)+\tfrac{1}{36}t_at_e(-5F_1+9F_2+2F_4)+\tfrac{1}{36}[t_a^2(-F_1+3F_2-2F_4)+t_e^2(23F_1+3F_2-2F_4)+2t_at_e(7F_1-3F_2+2F_4)][S(S+1)-\tfrac{3}{2}],$$

$$\langle[\mathrm{I}]\,{}^3E''({}^1E')|\mathbf{H}+\mathbf{V}_{\mathrm{trig}}+\mathbf{V}_C|[\mathrm{II}]\,{}^3E''({}^1E')\rangle=-\frac{\sqrt{2}}{3}\Delta+\frac{\sqrt{2}}{3}(U_2-U_1)+\frac{1}{36\sqrt{2}}[t_a^2(F_1+9F_2+2F_4)+t_e^2(-5F_1+9F_2-4F_4)+2t_at_e(2F_1-9F_2+F_4)]+\frac{1}{18\sqrt{2}}[t_a^2(-F_1+3F_2-2F_4)+t_e^2(5F_1+3F_2+4F_4)-2t_at_e(2F_1+3F_2+F_4)][S(S+1)-\tfrac{3}{2}].$$

The following notations for Coulomb integrals are used:

$$U_0 \equiv \langle x_0^A x_0^B \| x_0^A x_0^B \rangle = \int [x_0^A(1)]^2 \frac{1}{r_{12}} [x_0^B(2)]^2 d\tau_1 d\tau_2,$$

$$U_1 \equiv \langle x_\pm^A x_0^B \| x_\pm^A x_0^B \rangle,$$

$$U_2 \equiv \langle x_\pm^A x_\pm^B \| x_\pm^A x_\pm^B \rangle,$$

$$U_3 \equiv \langle x_\pm^A x_\mp^B \| x_\pm^A x_\mp^B \rangle.$$

[1] D. I. Khomskii and K. I. Kugel, Sov. Phys. Usp. **136**, 231 (1982).
[2] M. Drillon and R. Georges, Phys. Rev. B **24**, 1278 (1981).
[3] B. Leuenberger and H. U. Güdel, Mol. Phys. **51**, 1 (1984).
[4] J. J. Borrás-Almenar, J. M. Clemente-Juan, E. Coronado *et al.*, J. Phys. Chem. A **102**, 200 (1998).
[5] R. Saillant and R. A. D. Wentworth, Inorg. Chem. **7**, 1606 (1968).
[6] B. Briat, O. Kahn, I. Morgenstern-Badarau, and J. C. Rivoal, Inorg. Chem. **20**, 4193 (1981).
[7] G. J. Wessel and J. J. W. Ijdo, Acta Crystallogr. **10**, 466 (1957).
[8] M. Drillon and R. Georges, Phys. Rev. B **26**, 3882 (1982).
[9] O. Kahn, *Molecular Magnetism* (VCH, New York, 1993), p. 379.
[10] A. Ceulemans, G. A. Heylen, L. F. Chibotaru *et al.*, Inorg. Chim. Acta **251**, 15 (1996).
[11] A. Ceulemans, L. F. Chibotaru, G. A. Heylen *et al.*, Chem. Rev. **100**, 787 (2000).
[12] A. Ceulemans, L. F. Chibotaru, G. A. Heylen, and K. Pierloot, Mol. Phys. **97**, 1197 (1999).
[13] S. Sugano, Y. Tanabe, and H. Kamimura, *Multiplets of Transition Metal Ions in Crystals* (Academic, London, 1970).
[14] E. Clementi and C. Roetti, At. Data Nucl. Data Tables **14**, 177 (1974).
[15] J. E. Huheey, E. A. Keiter, and R. L. Keiter, *Inorganic Chemistry* (Harper Collins College, New York, 1993).
[16] L. B. Silver, *Irreducible Tensor Methods* (Academic, New York, 1976).
[17] J. S. Griffith, *The Irreducible Tensor Method for Molecular Symmetry Groups* (Prentice–Hall, Englewood Cliffs, 1962).
[18] D. A. Varshalovich, A. N. Moskalev, and V. K. Khersonskii, *Quantum Theory of Angular Momentum* (World Scientific, Singapore, 1988).
[19] B. S. Tsukerblat and M. I. Belinskii, *Magnetochemistry and Radiospectroscopy of Exchange Clusters* (Stiintsa, Kishinev, Moldova, 1983).
[20] A. Bencini and D. Gatteschi, *Electron Paramagnetic Resonance of Exchange Coupled Systems* (Springer-Verlag, New York, 1990).
[21] J. M. Clemente, A. V. Palii, T. S. Tsukerblat, and R. Georges, Exchange Interactions: II. Spin Hamiltonians, in *Molecular Magnetism: From Molecular Assemblies to the Devices*, edited by E. Coronado, P. Delhaès, D. Gatteschi, and J. S. Miller (Kluwer Academic, Dordrecht, 1996), Vol. E-321, pp. 85–104.
[22] B. S. Tsukerblat, *Group Theory in Chemistry and Spectroscopy* (Academic, London, 1994).
[23] J. J. Borrás-Almenar, J. M. Clemente-Juan, E. Coronado *et al.*, Chem. Phys. (submitted).
[24] P. W. Anderson, in *Magnetism*, edited by G. T. Rado and H. Suhl (Academic, New York, 1963).
[25] J. B. Goodenough, *Magnetism and the Chemical Bond* (Interscience, New York, 1963).
[26] B. Leuenberger, H. U. Güdel, and A. Furrer, Chem. Phys. Lett. **126**, 255 (1986).
[27] O. Kahn, Mol. Phys. **31**, 957 (1976).
[28] L. Chen, F. A. Cotton, K. R. Dunbar *et al.*, Inorg. Chem. **35**, 7358 (1996).